Spatio-temporal Characteristics of a Spray from a Liquid Jet in Crossflow

Scott Matthew Thawley

Thesis submitted to the faculty of the Virginia Polytechnic Institute and State University
in partial fulfillment of the requirements for the degree of

Master of Science
In
Mechanical Engineering

Dr. Uri Vandsburger
Dr. William Saunders
Dr. Jeffery A. Lovett

February 6, 2006
Blacksburg, VA

Keywords: two phase flow, liquid jet , combustion

Spatio-temporal Characteristics of a Spray from a Liquid Jet in Crossflow

Scott Matthew Thawley

ABSTRACT

A liquid jet in a crossflow is often used to as a fuel injection method for combustion systems. Parameters such as penetration and core trajectory are used as characterization for the spray and specification of design criteria for combustor geometry. In addition to penetration and core trajectory, mapping the mass flux in space and time is an important part of modeling evaporation and global equivalence ratio throughout the combustor. Accurate prediction of these spray characteristics allows for a stable and robust combustor design.

The break up of a liquid jet in a crossflow is an extremely complex phenomenon in both combination of mechanisms and variability of possible paths progressing from a liquid column to a distribution of individual droplets. In each region separate governing forces control the behavior of the liquid phase. Accordingly, different measurement techniques and different factors must be considered in each region.

Presented are the results of measurements using Phase Doppler Analyzer, PDA, and a time resolved, digital, particle imaging velocimetry system, TRDPIV. The measurements include instantaneous and time-averaged liquid phase velocity fields, spray penetration and core location in the near field and far field of the spray resulting from the liquid jet breakup.

With the TRDPIV system, the holistic properties of all three segments of a jet in crossflow were acquired with a single measurement. This allowed for comparison of system characteristics across not only individual pieces of one segment of the jet, for example PDA measurements of many droplets in one point of the far field spray, but characteristics across the entire system including the liquid column, near field spray, and far field spray simultaneously in a fashion that allowed for direct comparison between the different segments.

Acknowledgments

First, I would like to thank Dr Vandsburger, my adviser, for allowing me the opportunity to work towards my masters degree and for his support and direction during my work at Virginia Tech. I would also like to thank Dr. Saunders for helping me to start my masters and sitting on my committee. Jeff and Don both were helpful lending advice and experience. Special thanks to Jeff for being on my committee.

I would also like to thank David and Steve whom without the scope of this project would have been insurmountable. Thank you Steve for always being there for a new perspective, an answer about the lab, advice, and a helping hand. Thank you David for taking over the project while I spend the summer in Los Angeles on my UTSR internship, a whole semester of working with me to collect and process data, and giving me a reason to think that being at lab on a Saturday night is normal. The best of luck to both of you.

Although, Wajid and Prateep have graduated, working with them was a tremendous introduction to graduate school and has helped prepare me for the last few months of my degree. Also, Dr Baumann, Adam, Chris, Joe, and the rest of the CSDL for sharing their knowledge of other areas in combustion. Thank you to Dr. Vlachos and the students at the EFM lab for operating and teaching me to use the PIV system.

I would like to give a special thanks to the local machine shops, and construction companies that participated in the construction of the test section and work on the lab: Oliver White and the machinists at Damon Company, Wesley at Wesley Welding, Al and

Russel at Bentech, Reed Construction, and finally Joel and the welders at Hall's construction company. Everyone I met during the construction phase of my project was patient and helpful.

For reminding me that there are things in the world other then combustion and allowing me the opportunity to see and experience some of it, I would like to thank the YMCA and all of the people there. Through undergrad and graduate school, the Y has been the other half of my learning about life. Thank you.

Finally, I would like to thank my parents, Janet and Steven, for support and advice and a place to store my furniture and send my mail. With out my parents I would have nowhere to call home. Also, my sister has been a source of humor and a reminder that most people start a career after their first four years of college.

Illustration Index

Figure 1.1: Diagram of a Rayleigh instabilities on a liquid jet in quiescent gas..... 5
Figure 1.2: Digram and equations for force balance to predict liquid column cross-section shape and trajectory.....6
Figure 1.3: Time-averaged image with spray penetration and core trajectory at selected stream wise locations marked..... 9
Figure 2.1: Diagram of air and fuel/water supply.....19
Figure 2.2: Diagram of test section.....20
Figure 2.3: Diagram of PDA physical setup.....22
Figure 2.4: Diagram of TRDPIV physical setup..... 23
Figure 2.5: Negated example of an instantaneous digital image recorded with the PIV system..... 25
Figure 2.6: Instantaneous image of liquid jet in crossflow and corresponding mass averaged velocity field.....27
Figure 2.7: Map of averaged mass over the streamwise direction.....28
Figure 2.8: Map of instantaneous and average spray penetration hieght and core trajectory 30
Figure 2.9: Comparison of PDA normalized values for droplet diameter and liquid phase velocity.....31
Figure 3.1: Plot of the intensity summed in the vertical direction as a function of streamwise distance..... 33
Figure 3.2: Comparison of intensity plotted versus position and time..... 35
Figure 3.3: Example plot of frequency content in illumination of image case 7.....36
Figure 3.4: Frequency content of intensity maps for cases 2, 7, and 8.....37
Figure 4.1: Instantaneous and time-averaged velocity fields for case 1.....41
Figure 4.2: Instantaneous and time-averaged velocity fields for case 2.....42
Figure 4.3: Comparison of instantaneous velocity fields for cases 1 and 7 43
Figure 4.4: Instantaneous and average velocity fields for case 7..... 44

Figure 4.5: Instantaneous and average velocity field for case 8.....45
Figure 4.6: Instantaneous and time-averaged velocity field for case 4.....47
Figure 4.7: Instantaneous images of the liquid column for cases 3 (bottom) and 7 (top). 48
Figure 4.8: Instantaneous and average velocity field for case 5 (top) and case 6 (bottom).
.....49
Figure 4.9: Instantaneous identification of the spray penetration and core trajectory.....51
Figure 4.10: Instantaneous velocity field, spray penetration, and core trajectory for case 1.
.....53
Figure 4.11: Instantaneous velocity, penetration and core location for case 2.....54
Figure 4.12: Instantaneous velocity, penetration, and core trajectory for case 8.....54
Figure 4.13: Instantaneous velocity, penetration and core location for case 7.....55
Figure 4.14: Time-averaged velocity profile, spray penetration and core location for case
1.....57
Figure 4.15: Time-averaged velocity field, spray penetration and core location for case 2.
.....58
Figure 4.16: Time-averaged velocity field, spray penetration and core location for case 7.
.....58
Figure 4.17: Time-averaged velocity, spray penetration and core location for case 8..... 60
Figure 4.18: Comparison of penetration and core location.....61
Figure 4.19: Comparison of fluctuation amplitude for penetration and core height..... 62

Table of Contents

Acknowledgments....iv
Chapter 1 Introduction....1
1.1Motivation for Current Research....2
1.2Jet in Crossflow: Literature Review....3
1.2.1Liquid Jet Column....4
1.2.2Near Field Spray....8
1.2.3Far Field Spray....10
1.2.4Experimental Non-dimensional Parameters....12
1.2.5Literature Review Summary....14
1.3Research Objectives....15
Chapter 2 Experimental Setup and Measurement Methodology....17
2.1Design and Construction of Test Section....18
2.2Measurement System Configurations....21
2.3Data Processing....24
2.3.1PDA Data Processing....24
2.3.2PIV Data Processing....25
Chapter 3 Spatio-temporal Mass Fluctuations in the Spray....32
Chapter 4 Spatio-Temporal Velocity and Spray Characteristics....39
4.1Instantaneous Liquid-phase Velocity Field....40
4.1.1Cases 1 and 2: Water Jet at Ambient Temperature....40
4.1.2Cases 7 and 8: Kerosene in Heated Crossflow....43
4.1.3Cases 3, 4, 5, and 6: Water at High Weber Numbers and Low Reynolds Numbers....46
4.2Spray Penetration and Core trajectory....50
4.2.1Instantaneous Spray Penetration and Core Trajectory....50
4.2.2Overview of Individual Cases....53
4.2.3Time-averaged Results from Instantaneous Analysis....56

4.2.4Case Comparison.....60
Chapter 5 Conclusions and Future Work.....64
5.1Mass Fluctuations.....65
5.2Spray Characteristics.....66
5.3Recommendations for Future Work.....66
Bibliography.....69
Appendix A: Experimental Setup Details.....71
Appendix B: Test Section Details.....72
Appendix C: Measurement System Details.....77
Appendix D: Penetration Height and Core Location Identification.....78
Appendix E: Mass Fluctuation Program.....86
Appendix F: Data Collection and Processing Summary.....92
Appendix G: Data Collection Process.....96
Appendix H: Summary of Previous Work.....106

Chapter 1 Introduction

The study of a liquid jet in a crossflow involves not only the combination of numerous forces acting on the free, moving boundary of the liquid phase, but also a large number of individual particles all possessing different characteristics and different environments that act on them. Studies on this subject have chosen one of two paths. The first is to simplify the experiments to isolate a single element of the process and define the characteristics for the element over a range of operating conditions. The second path, which is followed in the current study, is to measure holistic characteristics of the entire process and attempt to understand the processes as a whole ignoring the details of how each particles behaves.

1.1 Motivation for Current Research

A liquid jet in a crossflow is often used to as a fuel injection method for combustion systems. Parameters such as penetration and core trajectory are used as characterization for the spray and specification of design criteria for combustor geometry. In addition to penetration and core trajectory, mapping the mass flux in space and time is an important part of modeling evaporation and global equivalence ratio throughout the combustor. Accurate prediction of these spray characteristics allows for a stable and robust combustor design. (Michou, Pichard, and Gokalp, 2000 and Chishty, 2005)

Much of the current data for a jet in crossflow is resolved for course grid spacing in space on a time-averaged basis. In the liquid column region, instability development has been studied for distances along the jet, but the convective liquid velocities carrying these instabilities have not been established. Lack of convective liquid velocities makes the association of fluctuations in the liquid column difficult to match to fluctuations in the spray. In the near and far fields of the spray time-averaged quantities are primarily used due to the limitations of the most popular methods for data collection such as Phase Doppler Anemometry and time-averaged Mie scattering or streak photography.

Time-averaged data, while useful, misses information about important time-dependent behavior and fluctuations of the spray. Fluctuations in spray characteristics such as mass flux and penetration can lead to fluctuations in global equivalence ratio, changes in droplet diameters distributions, and changes in the cross-sectional area

containing liquid. Fluctuations in any of these characteristics can also drive instabilities in flame fronts, or effect the accuracy of mixing and evaporation models. Although spreading of the spray and diffusion of the gaseous fuel will damp out fluctuations, instabilities in the liquid column can propagate downstream through the near field and into the far field regions of the spray. With the current trend to make combustors smaller and burn lean, fluctuations in the spray are more likely to reach the flame front possibly causing higher emissions, lower efficiency, flame out, or flashback.

1.2 Jet in Crossflow: Literature Review

Jet in crossflow breakup is divided into three segments: liquid column, near field or dense spray, and far field spray. Each segment has unique characteristic forces governing disintegration and breakup from a single liquid column into a distribution of spherical droplets. The balance of these forces governs the resulting sizes and distribution of droplets in the far field. Together these three regions contain the evolution of a liquid jet in a cross flow from the end of the internal flow in the orifice to individual droplets evaporating and reaching the flame front of a combustor. Furthermore, descriptors of the experimental conditions with clear relationship to the evolution of the jet in crossflow have been established and are used to compare experiments.

1.2.1 Liquid Jet Column

The liquid column segment of a jet in a crossflow begins at the exit of the injector orifice. At this boundary the liquid column properties of concern are the internal velocity field and relevant liquid properties. The liquid column segment continues into the perpendicular gas flow where it deforms and grows unstable until the surface instabilities reach an amplitude large enough to pinch off the end of the jet. The pinch point marks the end of the liquid column segment. (Sallam, Aalburg, and Faeth,2004)

Instability mechanisms and trajectory constraints of the liquid column include the balance of liquid surface tension and viscous forces, discontinuous boundaries at the orifice exit, aerodynamic drag forces, and interaction at the liquid-gas interface. Although much work has been done to quantify the effects of each mechanism, more work is required to create a complete model that describes the behavior of a free liquid jet in crossflow across all regimes of breakup.

Rayleigh (1878), was one of the first to study the instability of a liquid column. By studying a low velocity liquid column in quiescent air, Rayleigh was able to isolate the liquid surface tension forces and balance them with pressure forces. He concluded that perturbations in the column would produce swelling and constriction that would grow in amplitude if larger then the circumference of the liquid column. Also, for high speed liquid jets, Inamura (2001) proposed that turbulence and fluid structures inside the jet, characterized by the liquid column Reynolds number, was the dominating factor for liquid column instability. Using a numerical model Inamura determined that liquid

turbulence was the main cause of the initial liquid column disturbance, which would then propogate by Rayleigh's criteria. He then proposed that the effect of the gas was solely to amplify these disturbances.

Figure 1.1 shows diagram of a liquid jet breaking due to the Rayleigh instability.

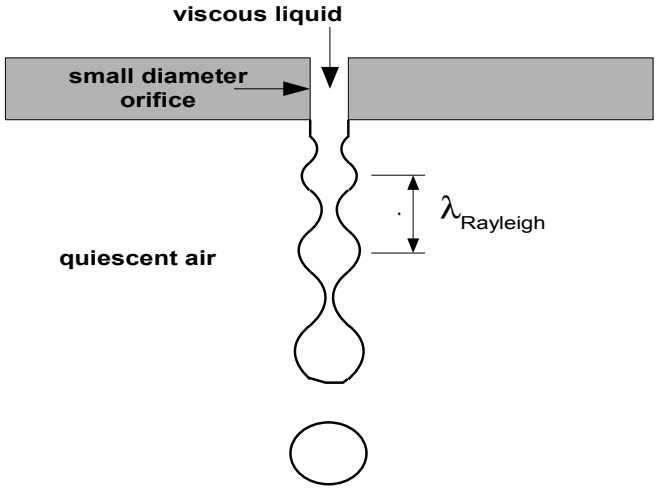

Figure 1.1: Diagram of a Rayleigh instabilities on a liquid jet in quiescent gas.

Discontinuous boundary conditions at the orifice exit have also been shown to cause a swelling of the liquid column at the exit of the orifice. Hillbing and Heister (1989) numerically modeled the liquid jet exiting a circular orifice ignoring all gas effects on the jet. The model predicted a swelling in the liquid column as it exited the orifice and a change from a boundary layer bounded by a no-slip solid wall to a shear layer at

the free liquid-gas interface. Together the boundary and internal flow changes initiated instabilities in the liquid column. Results from the study showed that liquid column instabilities could exist solely due to the discontinuous change in boundary conditions.

The gas effect on the cross-sectional area of the liquid column was modeled by Inamura (1999). Results from both studies show deformation from a circular cross-sectional shape at the orifice to an ellipse shape, due to the system of viscous and surface tension forces actuated the external pressure force from aerodynamic effects. Figure 1.2 shows the force balance Inamura used to predict the deformation and trajectory of the liquid column. The balance between the position of the liquid column and viscous, surface tension, plus forcing by the external pressure was conducted on successive slices of the liquid column. The solution to this balance yielded the liquid column trajectory in addition to the cross-sectional shape.

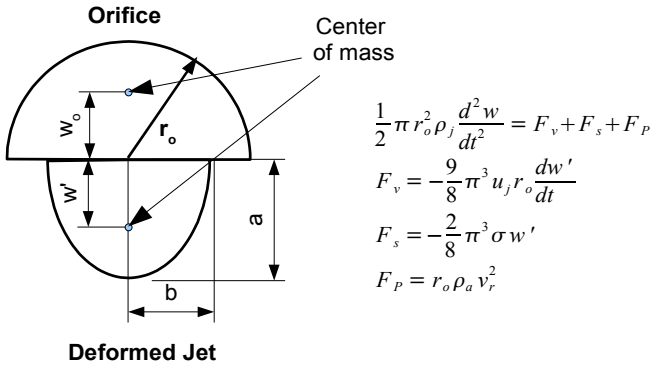

Figure 1.2: Digram and equations for force balance to predict liquid column cross-section shape and trajectory.

The first equation is the balance between the center of mass, w, movement and applicable forces. F_v is the viscous force in the jet, F_s is the surface tension force, and F_P is the pressure acting on the jet surface due to the airflow. The center of mass position is denoted as w in the equations with the prime indicating the next center of mass position. The liquid jet properties used are the density, ρ_j , and viscosity, μ_j. The orifice radius, r_o, and the air properties; density, ρ_a, and velocity, v_a, are also included in the force balance. (Inamura, 1999)

Effects of gas flow on the liquid column surface were studied. Less and Schetz (1986) measured the frequency of surface waves on the liquid column using a laser extinction measurement system to demonstrate that the wave number of surface instabilities varied as a function of only air velocity and orifice diameter.

Finally the instabilities inherent in a gas-liquid free surface interface can be described by the criteria of the Kelvin-Helmholtz instabilities. This instability occurs on free surface liquid-gas surfaces. Varga Lasheras and Hopfinger (2003) outline the Kelvin-Helmholtz instability and the Rayleigh-Taylor instability illustrating their interaction for a liquid jet in co-flowing air Varga, Lasheras, Hopfinger, 2003). A similar study by Mayer and Branam (2004) was conducted that highlighted effects of gas velocity, pressure, and liquid velocity on surface wave. Both studies demonstrate how instabilities grow along the jet surface until the amplitudes of the resulting surface waves are large enough to fracture the liquid column, but both studies are limited to liquid jets in co-flowing air.

For jet in a crossflow, parameters such as relative velocity, between liquid and gas, and acceleration of the liquid column are not straight forward due to the bending of the jet. Work to measure the resulting frequencies due to the instabilities has been conducted to relate the frequency of liquid column breaking to the frequency of surface waves. The results showed that the frequency of liquid column breaking was a function of gas velocity and orifice diameter. (Less, 1985)

1.2.2 Near Field Spray

The near field spray region begins at the disintegration of the liquid column and continues through the region of spray that contains liquid clumps broken from the end of the liquid jet and ligaments shed from the jet circumference. The evolution of a liquid continues when the clumps and ligaments break up into smaller spherical droplets and the mean space between droplets increases to where the droplets do not interact. These processes' completion designates the end of the near fields spray region. The work that has been conducted in this region of the spray is usually holistic or qualitative because many of the liquid particles are non-spherical and the space between particles is on the same order of magnitudes as the size of the particles creating problems with interference and noise.

Because of the problem of quantifying individual droplets in the near field region, holistic spray characteristics such as penetration and mass flux distribution are used to

describe the spray behavior in this region. An example of jet penetration and mass flux distribution is shown in Figure 1.3.

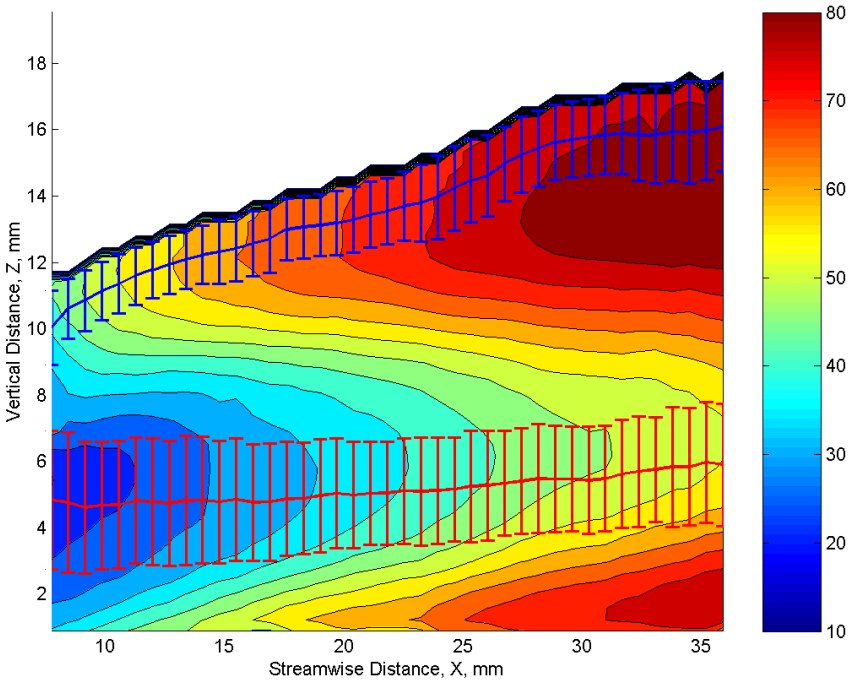

Figure 1.3: Time-averaged image with spray penetration and core trajectory at selected stream wise locations marked.

Streak and instantaneous photography has been used to measure jet penetration and describe qualitative characteristics of the near field spray (Schetz and Padhye, 1977 and Becker and Hassa, 2002). Chen, Smith and Schommer (1993) reviewed penetration correlations and compared them with data collected using a two-dimensional imaging system to acquire light scattering intensities from the spray. The basic functional form of penetration suggested by Chen's work is

$$\frac{H}{d_o} = A(\bar{q})^n \left(\frac{x}{d_o} \right)^m$$

where H is the penetration, d_o is the orifice diameter, q is the momentum ratio, x is the streamwise location, and *A, n, and m* are data correlated coefficients. Inamura and Nagai's (1997) experiments using an isokenetic sampling probe arrived at a similar relationship for jet penetration.

Overall, time-averaged jet penetration trajectory and mass flux have been studied over a wide range of experimental conditions in the near field. A variety of measurements techniques have been used and all of the studies have yielded a similar form for the correlation between flow descriptors such as aerodynamic Weber number, momentum flux ratio, and gas Reynolds number. Also, the trajectories found in the near spray are similar to the trajectories predicted for the liquid column itself. In addition to time-averaged characteristics, some studies have illustrated instantaneous variability in the spray formed from a liquid jet in crossflow, but quantitative description of instantaneous jet characteristics has yet to be identified.

1.2.3 Far Field Spray

The far field region of the spray begins when all of the clumps and ligaments in the spray have broken down into small spherical droplets. In this region of the spray, Particle Doppler Anemometry, PDA, has been successfully employed to identify time-averaged spray characteristics, droplet size and velocity distributions throughout the

spray (Becker and Hassa, 2002). Green, Nejad, and Roe (1994) completed a study of droplet velocities and size in planes perpendicular to the flow and in the streamwise direction. The data collected identifies penetration heights and the core of the spray using these velocity and diameter distributions over space.

Due to the sparse distribution of droplets, many researchers study the behavior of individual droplets. Experiments encompassing a broad range of gas flow and liquid property conditions have been conducted by Aalburg, vanLeer, and Faeth (2003). Detailed analysis of the breakup processes for a single liquid drop in a gaseous medium and the transitions between different breakup regimes were outlined by Aalburg, vanLeer and Faeth.

1.2.4 Experimental Non-dimensional Parameters

For a jet in a crossflow experiments four major parameters are often used to describe the conditions. These four parameters are the jet momentum ratio, the gas phase Reynolds number, and aerodynamic Weber number and the Ohnesorge number. Together these four parameters give a description of the experiment that includes most of the major governing forces and reactions of the jet to these force.

The jet momentum ratio is the ratio of the momentum of the air over the momentum of the jet in the fashion shown below

$$q = \frac{\rho_g U_g^2}{\rho_l U_l^2}$$

where q is the momentum ratio, ρ and U are the density and velocity respectively, and the subscript g represents the gas phase, and l represents the liquid phase. The jet momentum ratio effects all segments of the jet and is often used in correlations as a scalable, non-dimensional parameter to compare results across experiments.

The second parameter, aerodynamic Weber number is the ratio of air momentum and the liquid phase surface tension. Aerodynamic Weber number is a significant parameter often used to describe the rate of breakup for the liquid column and far field droplet diameter distribution. The aerodynamic Weber number is defined as:

$$We_g = \frac{\rho_g U_g^2 d_o}{\sigma_l}$$

where, as before, ρ_g and U_g are the gas phase density and velocity. The jet orifice diameter, d_o, and the liquid phase surface tension, σ_l, are used as characteristics of the jet.

The third parameter, gas phase Reynolds number, Re_g, is widely used through out fluid dynamics to characterize the turbulence and energy of a flow in a scalable, non-dimensional fashion. The gas phase Reynolds number is defined as:

$$\mathrm{Re}_g = \frac{\rho_g U_g d_g}{\mu_g}$$

where the gas density and velocity are signified as ρ_g and U_g and the gas phase viscosity is signified as μ_g. The characteristic length for the current experiments was set to the channel height, 5.08 cm, which is represented as d_g in the above equation.

The fourth parameter, the Ohnesorge number, describes solely liquid phase characteristics. The Ohnesorge number, Oh, is the ratio of viscous forces to the square root of inertial forces and surface tension forces in the form:

$$Oh = \frac{\mu}{\sqrt{\rho d_o \sigma}}$$

where μ is the liquid viscosity, ρ is the liquid density, σ is the liquid surface tension, and d_0 is the orifice diameter. The rate of momentum exchange and the ability of the liquid jet to become unstable are described using the Ohnesorge number.

These four parameters will be used in the following study to compare varying experimental conditions in a scalable, non-dimension fashion. Some studies use the jet Weber number as an experimental descriptor, but by using both the momentum ratio and Ohnesorge number, the key factors in the jet Weber number will be covered. One factor not covered by these parameters is the velocity profile and turbulence level of the liquid column inside of the orifice. Often investigators design the length over diameter of the orifice and the reservoir feeding the orifice in such a manner as to insure fully developed pipe flow at the exit of the orifice. For reasons specific to this study, not all of the proper precautions were included in the experimental geometry and therefore comparison of the current data to existing data is not included.

1.2.5 Literature Review Summary

The break up of a liquid jet in a crossflow is an extremely complex phenomenon in both combination of mechanisms and variability of possible paths progressing from a liquid column to a distribution of individual droplets. In each region separate governing forces control the behavior of the liquid phase. Accordingly, different measurement techniques and different factors must be considered in each region.

Although the characteristics of each region are different, throughout all of the regions the prominent phenomena studied have been successfully related to four non-

dimensional flow descriptors: momentum ratio, aerodynamic Weber number, Ohnesorge number, and the gas phase Reynolds number.

With the theoretical knowledge and data collected by previous researchers, demonstration of the characteristics of liquid column instabilities and the forces that govern their behavior have been outline. Using these characteristics and information from previous results, summarized in Appendix H,the search for the effects of instabilities in the liquid column on the spray can be conducted in a straight forward manner.

1.3 Research Objectives

The goal of the present study is to identify the time average and fluctuating components of the jet in crossflow characteristics in the near and far field spray segments. Particularly the characteristics used to describe these segments are the spray penetration, core trajectory and averaged mass fluctuations in the streamwise direction.

The identification and comparison of liquid jet in a crossflow characteristics for varying experimental conditions includes 6 tasks:

1) Design and construction of a test section

2) Measurement system assembly and data collection

3) Identification of instantaneous and time-averaged liquid phase velocity fields

4) Identification and analysis of instantaneous and time-average spray characteristics at each experimental condition (penetration, core trajectory and averaged mass flux)

5) Examination of amplitude and frequency components of the spray characteristics

6) Comparison of spray characteristics for different conditions and examination of changes in spray characteristics to experimental descriptors (aerodynamic Weber number, momentum flux ratio, and Ohnesorge number)

Tasks 3, 4, and 5 were demonstrated for the text conditions presented below in Table 1.

Case number	***Liquid***	***Air Velocity m/s***	***Air Temp K***	***Momentum ratio q***	Re_g	We_g	***Oh***
1	water	75	294	12	271,000	92	0.0067
2	water	100	294	12	1,185,000	165	0.0067
3	water	137	394	12	305,000	232	0.0067
4	water	137	394	18	305,000	232	0.0067
5	water	137	755	12	103,000	121	0.0067
6	water	137	755	18	103,000	121	0.0067
7	kerosene	137	394	12	305,000	138	0.0078
8	kerosene	137	394	18	305,000	138	0.0078

Table 1: Table of experimental conditions.

Chapter 2 Experimental Setup and Measurement Methodology

In order to characterize the physical phenomena occurring during the evolution of a liquid jet in a gaseous crossflow, an optically accessible test section, a plain orifice injector, and an incinerator were constructed. The test section was made optically accessible on three sides to allow measurements using time resolved digital particle imaging velocimetry, TRDPIV, and phase Doppler anemometry,PDA. Instantaneous and time averaged data from the TRDPIV system and time averaged data from the PDA system were then processed and interpreted to map physical phenomena of the jet in crossflow experiment over space and time. The following sections will present details of the test section construction, description of the measurement device setups, and an outline of the processing methods used to produce the results of the current study.

2.1 Design and Construction of Test Section

For the results presented in this thesis, an experimental setup capable of an air velocity of 140 $^{m}/_{s,}$ an air temperature of 755 K, and a jet momentum ratio up to 30 was required. An 8 inch diameter cylindrical to a 2 x 5 inch rectangular convergence section, optically accessible rectangular test section, and an incinerator section were constructed to fit into an existing modular combustion facility. Figure 2.1 shows a diagram of the facility supplying air and fuel to the test section. Details of the system components are given in Appendix A.

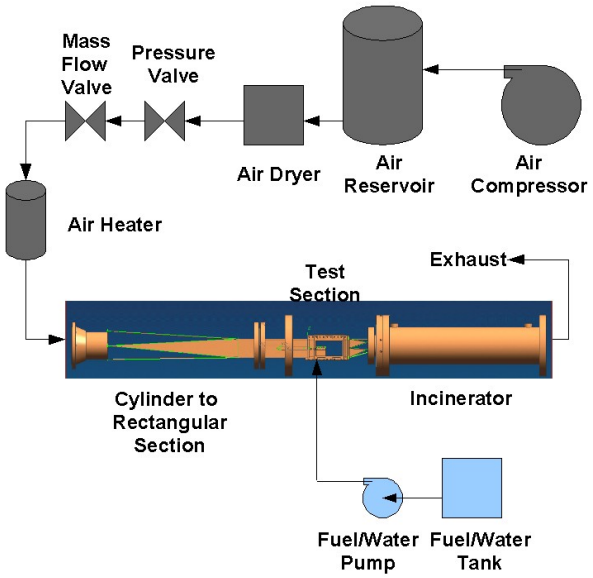

Figure 2.1: Diagram of air and fuel/water supply

The test section was designed to give a flat velocity profile with a boundary layer of approximately 2 mm at the orifice where the liquid jet is injected perpendicular to the flow. As shown in Figure 2.2, optical access was present on both sides and from the top of the test section. The optical access starts 2.54 cm upstream of injection and reaches 6 inches downstream and 4.45 cm above the surface of the vane. In addition to the optical access, ports for Pitot tubes, static pressure port, and thermocouples were place 8.89 cm and 40 cm upstream of the orifice.

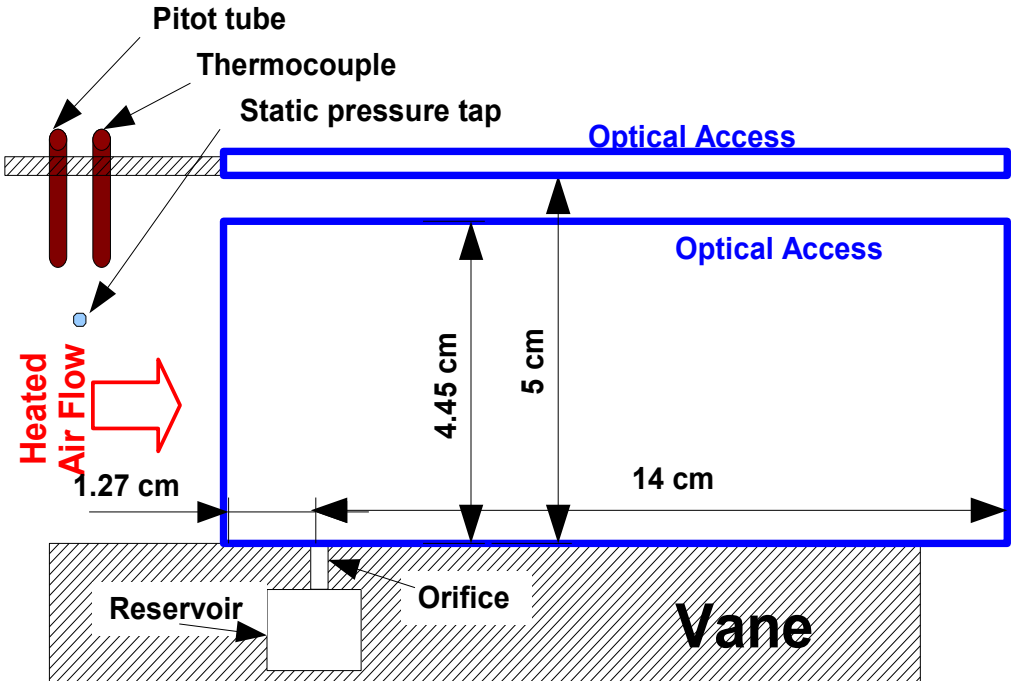

Figure 2.2: Diagram of test section.

The optical access allowed for measurement over the height of the spray at the centerline and enough distance in the flow direction to capture the liquid column, near and far field segments of the jet in crossflow for all the experimental conditions presented.

For the experiments using kerosene, an incinerator was required to burn the injected fuel. After the air and fuel exited the test section they converged to a 4" circular orifice and then entered the incinerator. The incinerator is a dump combustor with a 4" inlet to an 8" dump and a flame holder just upstream of the dump as illustrated in Figure 2.6. The flame holder was installed to shorten the flame length and to increase flame stability.

The flame is stabilized with methane injected 14 cm upstream of the dump plane and ignited using a spark plug with premixed propane injected into the dump region. After the air exits the post combustor it enters a water spray section that cools the air to a temperature safe for exhausting. More detail about the experimental hardware is included in Appendix B.

2.2 Measurement System Configurations

The experiment setup requirs access for both Phase Doppler anemometry, PDA, and time resolved digital particle imaging velocimetry, TRDPIV or PIV, systems with the ability to quickly change from one measurement system to the other. Described below are the details of each system separately and then a short description of how the two systems were overlaid.

The PDA system simultaneously measures droplet diameter and velocity using the phase shift and frequency shift of reflected or refracted light from a fringe pattern created by crossing two coherent laser beams. The laser crossing creates a fringe pattern over a small volume where, per the method developed by Bachalo and Hauser (1984), droplet

velocity and diameter is measured. The small measurement volume, formed by the laser beam crossing, is placed in the spray with the fringes perpendicular to the flow direction. The receiving optics for this experiment were placed at a forward scattering angle of 25^0 to maximize absolute scattering intensity. Three photo multipliers then record the total refraction reaching to receiving optics over time. The frequency and phase from the three photo multipliers are then compared to obtain the velocity and size of the droplets as they pass through the measurement volume. Figure 2.3 shows a diagram of the PDA setup used for all of the results contained herein. Specifics of the PDA system are listed in Appendix C. (Bate and Ayob, 1995)

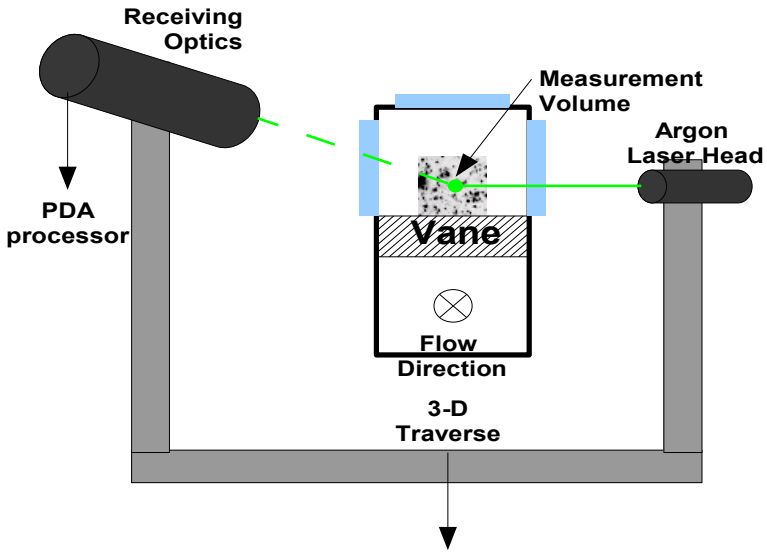

Figure 2.3: Diagram of PDA physical setup

Two different TRDPIV systems were used. The specifics of each of these systems are detailed in Appendix C The instantaneous pictures were taken in pairs with a

separation of 2 μs at a rate of 15 Hz or 500 Hz. These instantaneous pictures were recorded for further processing of local velocity and relative mass flux.

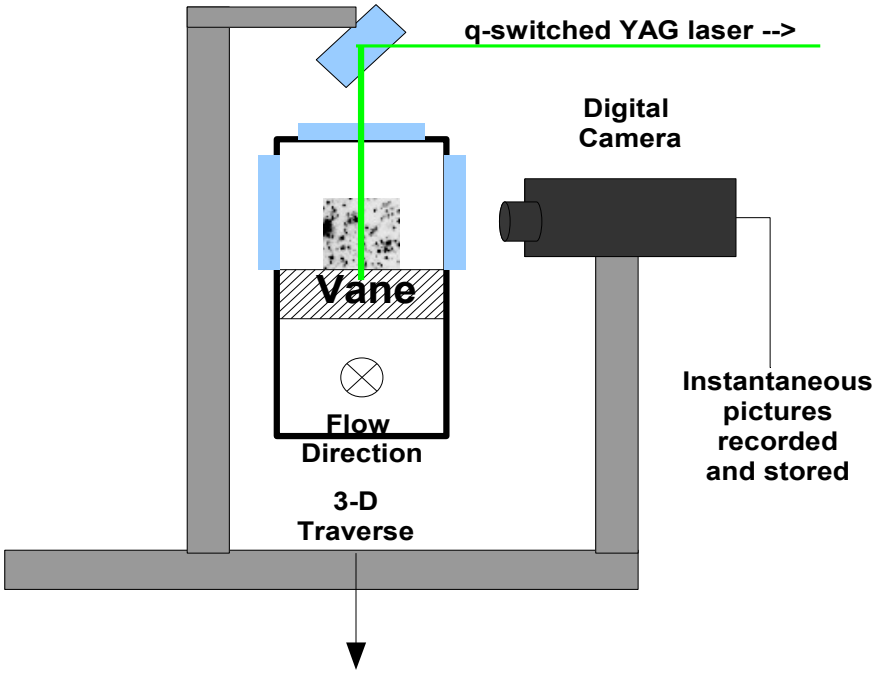

Figure 2.4: Diagram of TRDPIV physical setup

The lasers, power supplies, computers, and triggering hardware were placed on an optical table next to the experiment. The optics required to direct the lasers from the optical table to the experiment, the camera, and the PDA optics were mounted to a single traverse built below the experimental centerline. The PDA optics were mounted to the same rigid aluminum arm as the TRDPIV instrumentation but at a nominally higher position so changing from one measurement system to the other required only moving the

traverse vertically. This also allowed for the alignment of the optics with minimal work required when the systems were switched.

2.3 Data Processing

Although both the PDA and PIV systems record raw data, the data from the PDA is converted from a Doppler signal to droplet size and velocity by the processor hardware and only these statistics are recorded during the experiment. On the other hand, the PIV system records only a digital image which requires post-processing to obtain useful information from the raw data. The next two section detail the methods used to process information recorded by each measurement system.

2.3.1 PDA Data Processing

The raw data from the PDA system at the time of experiment is saved in the form of a list of a particle's diameter, velocity, and time of arrival at each spatial location in the spray over the collection time. The collection time is restricted by user defined limits of particles, 10,000 for the current study, or maximum collection time, 100 s for the current

study. For the current study only the mean velocity and mean droplet diameter at each location are considered.

In the case of the mean velocity, the one-dimensional velocity of each droplet collected was averaged at each spatial location. For analysis based on droplet diameter the Saunter Mean diameter of all of the droplets collected for each location was used to determine a representative diameter at each measurement location. Than a profile of Saunter mean diameters at a single streamwise location was established.

The Saunter mean diameter is the total surface area of the droplets divided by the total volume of the droplets. Taking the mean in this manner allows for a single value to represent the mean based on volume instead of simply number density. This is beneficial for two phase flow, because mass in a more pertinent parameter then number of droplets.

2.3.2 PIV Data Processing

The PIV system records an 8-bit gray-scale digital image at the time of the experiment. All of the images require post-processing in order to yield droplet and spray

Figure 2.5: Negated example of an instantaneous digital image recorded with the PIV system

information. The information of interest for the current study is frequency of fluctuation for the average mass flux in the streamwise direction, spray penetration height, and spray core trajectory. A negated example of the images used to evaluate the spray characteristics is displayed in Figure 2.4.

Following the method described by R.J. Adrian (1991), 2-dimensional velocity vectors were calculated for each point in a user defined grid throughout the spray. Per Adrian's method, two instantaneous images are broken up into matching blocks. Then these blocks are cross-correlated to identify the displacement that best represents the motion of the particles in that block. This displacement is then divided by the time separating the two instantaneous images to yield the local velocity. For the current study, the exposure time for each instantaneous image was 10 ns and the time between images in a pair was 2 μs. A second order, discrete window offset algorithm with a normalized FFT based correlation method was used to evaluate the velocity for the current study (Abiven and Vlachos, 2002). Fifteen hundred pairs of instantaneous images were recorded to be used in the following analysis. Figure 2.5 show an example of the velocity field yielded.

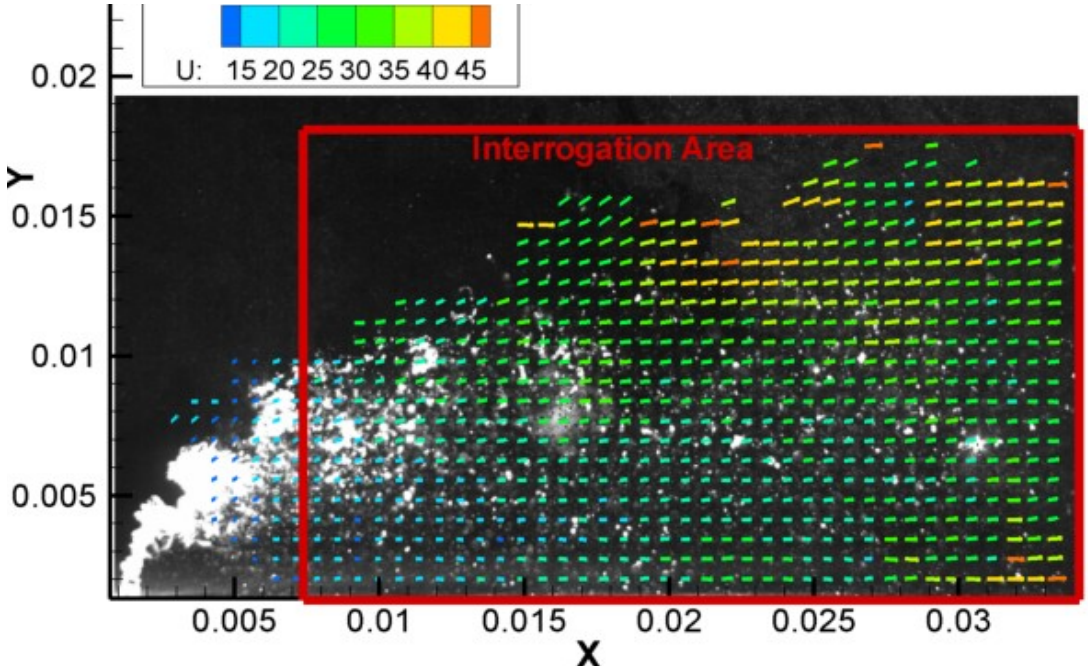

Figure 2.6: Instantaneous image of liquid jet in crossflow and corresponding mass averaged velocity field.

The relative change in mass flux was mapped by first collapsing the two dimensional image into a one dimension by summing the intensities in the vertical, z, direction . The sum at each pixel in the x direction was then averaged with the next 15 pixels in order to filter out the high frequency noise produced by the space between droplets.

Based on light scattering principles the amount of light refracted from the laser sheet 90^{o} to the camera lens is proportional to the volume of the droplets (Bate and Ayob, 1995). For simplicity the density of the liquid phase is assumed to be constant. Therefore, the intensity is proportional to volume which , in turn is proportional to mass.

Figure 2.6 shows an example of the mass fluctuations overlaid on an instantaneous image. After the mass fluctuation was quantified, streamwise distance was converted to droplet residence time. After the fluctuation of mass were established as a function of time, an unsteady FFT was performed to identify the major frequency of fluctuations using the Lomb Peridiogram (Press et al., 1992).

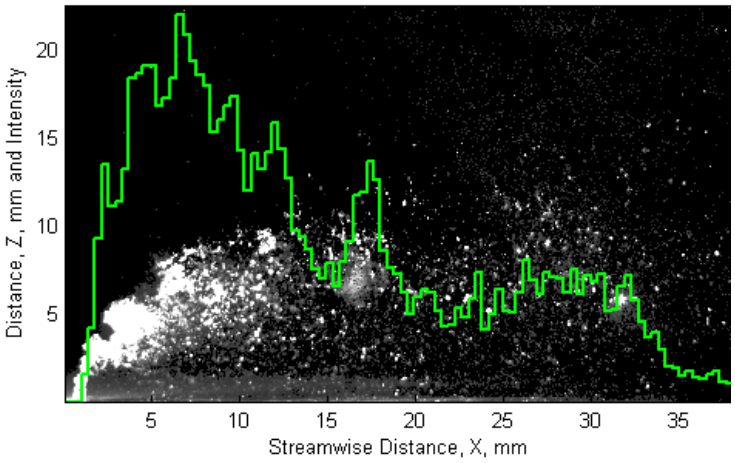

Figure 2.7: Map of averaged mass over the streamwise direction.

Lomb Peridiogram performs a spectral analysis of unevenly sampled data. The method calculated the power for a frequency ω using the following equation;

$$P_N(\omega) = \frac{1}{2\sigma^2}\left(\frac{\left[\sum_j (h_j - \bar{h})\cos\omega(t_j - \tau)\right]^2}{\sum_j \cos^2\omega(t_j - \tau)} + \frac{\left[\sum_j (h_j - \bar{h})\sin\omega(t_j - \tau)\right]^2}{\sum_j \sin^2\omega(t_j - \tau)}\right)$$

where

$$\tan(2\omega\tau) = \frac{\sum_j \sin 2\omega t_j}{\sum_j \cos 2\omega t_f}$$

For the above equation $\bar{h}$ is the mean of the data, h_j is the difference of a value at time t_j, and j is an index to represent the time at which the data was sampled. The constants in the equation are σ^2 which is the variance of the data and τ, an offset that makes the function independent of the start time. When the Peridiogram is iterated over a user defined range of frequencies a power spectrum results. (Press et al., 1992)

In addition to the fluctuation of mass in the spray, the penetration height and core location in the spray also fluctuate. For the penetration and core location, the amplitude of fluctuation will be the focus instead of the frequency. Spray penetration height is the distance from the surface containing the orifice to the highest vertical location that contains liquid. The method of identification for the penetration used, is counting the number of grid points with a streamwise velocity between 5 m/s and 90% of the free stream velocity. The current data set contains measurements of just spray and of spray and seeding together requiring both an upper and lower boundary to demarcate the edge of the spray. Because the PIV algorithm determines the most probable velocity in the interrogation block, the velocity of the droplets will dominate until the liquid mass fraction in the block is insignificant. An accuracy of one grid point, or approximately half of a jet diameter was achieved using this method. For each pair of images, the spray penetration was found at each x-location on the grid. The results for all 1500 image pairs were then combined to yield a mean and standard deviation of spray penetration for each x-location and each experimental condition. The standard deviation indicates the root

mean squared, RMS, amplitude of fluctuation in the penetration. Figure 2.8 displays an average field with the spray penetration height and core trajectory mapped out.

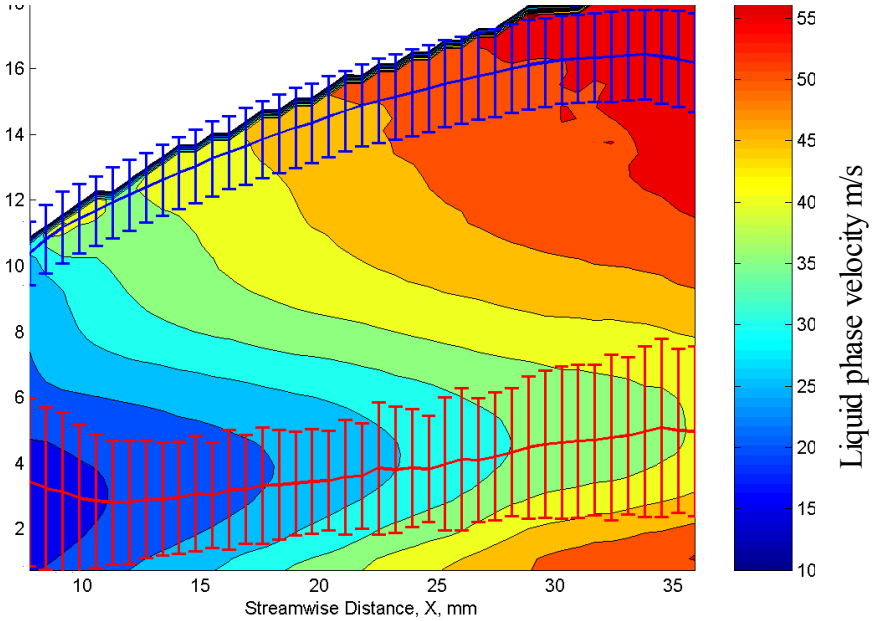

Figure 2.8: Map of instantaneous and average spray penetration hieght and core trajectory

The spray core trajectory was found in a similar manner. Figure 2.9 shows that the location of the lowest liquid phase velocity coincides with the location of highest Saunter mean droplet diameter. The highest mass flux and lowest liquid phase velocity coincide for two reasons. First, the inertia is proportional to droplet diameters squares and inversely proportional to acceleration. So, the largest droplets will accelerate the slowest and therefore have the lowest local velocity. Second, the spray core is usually the residual of breaking in the liquid column, so much of the mass in the spray core was

attached to the liquid column for the longest period of time, in essence giving droplets in other regions more exposure time to the air flow. Using the knowledge that the highest droplet diameter, and lowest liquid phase velocity coincided allowed the use of the instantaneous velocity field yielded by the PIV algorithm to map the spray core region and trajectory along the evolution of the spray in the streamwise direction. As with the penetration, the core trajectory at each streamwise grid location was identified for each image pair and then compiled to give and average and 95% confidence interval.

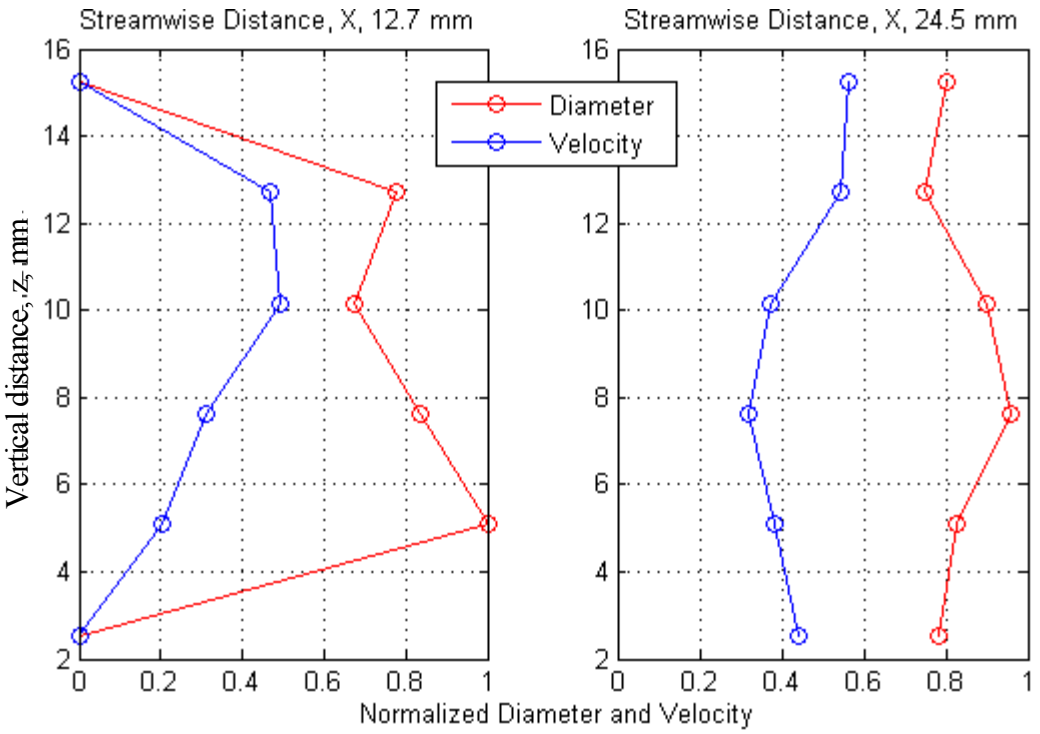

Figure 2.9: Comparison of PDA normalized values for droplet diameter and liquid phase velocity.

Chapter 3 Spatio-temporal Mass Fluctuations in the Spray

Instabilities in the liquid column cause the liquid column to pinch and break in a fluctuating manner. When the liquid column breaks, a large clump of liquid is detached from the end and travels down stream. The action of clumps breaking from the end of the jet causes a large change in the amount of mass separated from the liquid jet at that instant. The mass from the jet, in turn, enters the spray causing a similar fluctuation of mass. Using the PIV system, capturing both the breaking of the liquid column and a streamwise comparison of mass in the spray was possible. Using this measurement,the evolution of the clump after it breaks from the liquid column can be tracked as it travels downstream.

For this study, the amount of liquid mass in the spray at a streamwise locations were compared by relating the mass in the measurement plane to the intensity of light scattered. Because the only characteristic of interest was the rate at which the fluctuations occur, many of the complexities of light scattering analysis were avoided. The process used for the current study included taking one image from each image pair and running a basic threshold on it to eliminate noise. Then the intensity at each pixel in the vertical, z, direction was summed across the entire image and the average intensity of 16 neighboring pixels was averaged to eliminate high frequency noise. This process resulted in a signal similar to the one overlaid on an instantaneous image in Figure 3.1

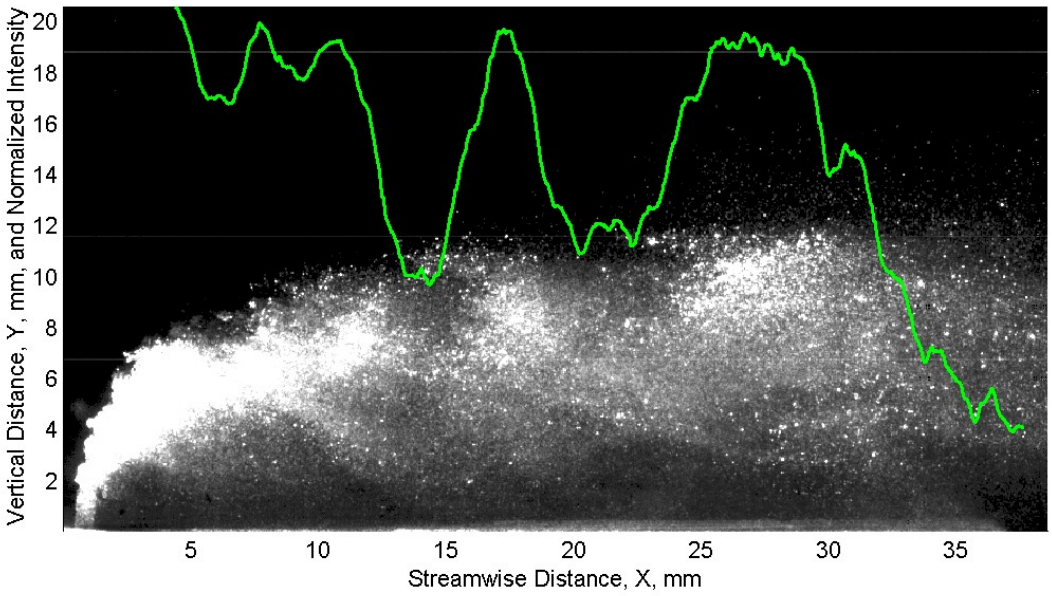

Figure 3.1: Plot of the intensity summed in the vertical direction as a function of streamwise distance.

The next step of processing the image was to convert the streamwise distance to a representative time. The time required to travel from the liquid column to the location where it is captured by the image has been labeled the droplet residence time. The droplet residence time was found by integrating the vertically and time averaged velocity field from the beginning of the interrogation area to the droplets current streamwise position. The slope of the velocity compared to streamwise distance was linear suggesting a constant acceleration of the spray as an averaged whole. The acceleration for the spray was calculated using the velocity at the upstream and downstream edges of the interrogation window. With the acceleration calculated, the time at each streamwise location could now be determined and used as the representative time between high and low points in the spray height average mass flux. Figure 3.2 shows an example of the change in shape of the intensity plot with the variable transformation.

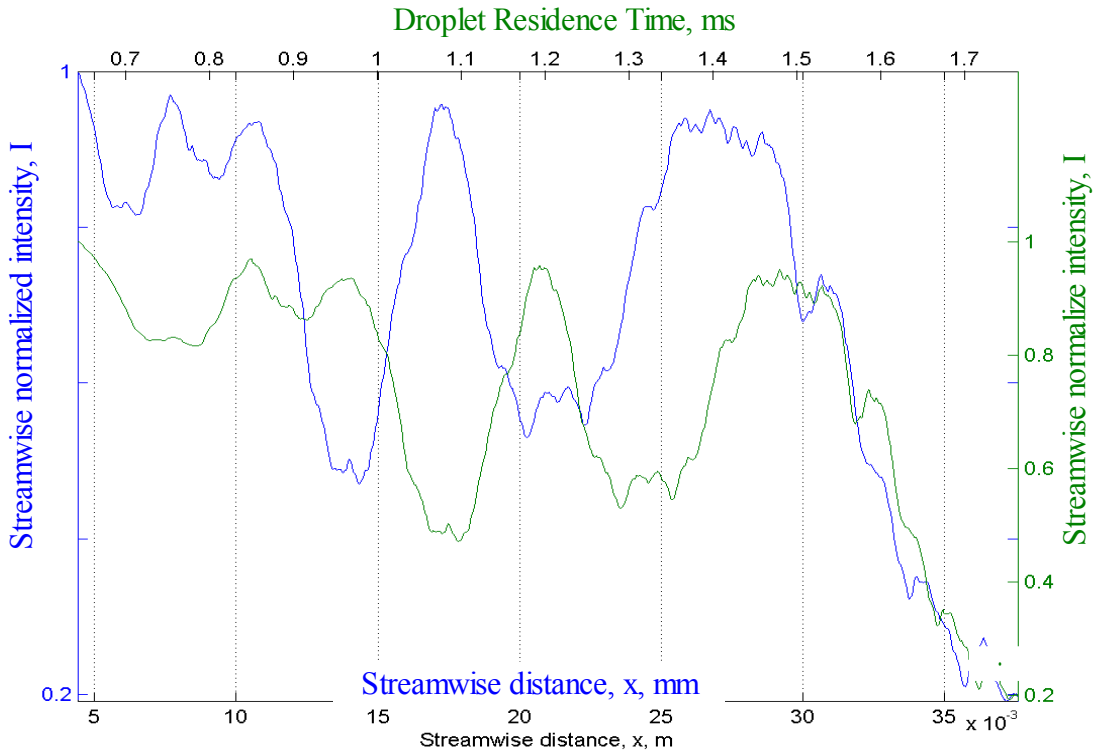

Figure 3.2: Comparison of intensity plotted versus position and time.

Using the image intensity and the droplet residence time the frequency content of the image was extracted using Lomb's Peridiogram (Press et al., 1992). Lomb's Peridiogram maps the power spectrum for unevenly sampled data over a user defined range of frequencies. Figure 3.3 shows an example of the output from Lomb's Peridiogram applied to a single image. The plot shows frequency content near 1600 Hz, which is in the range expected for liquid column in a cross flow for similar conditions (Less, 1985).

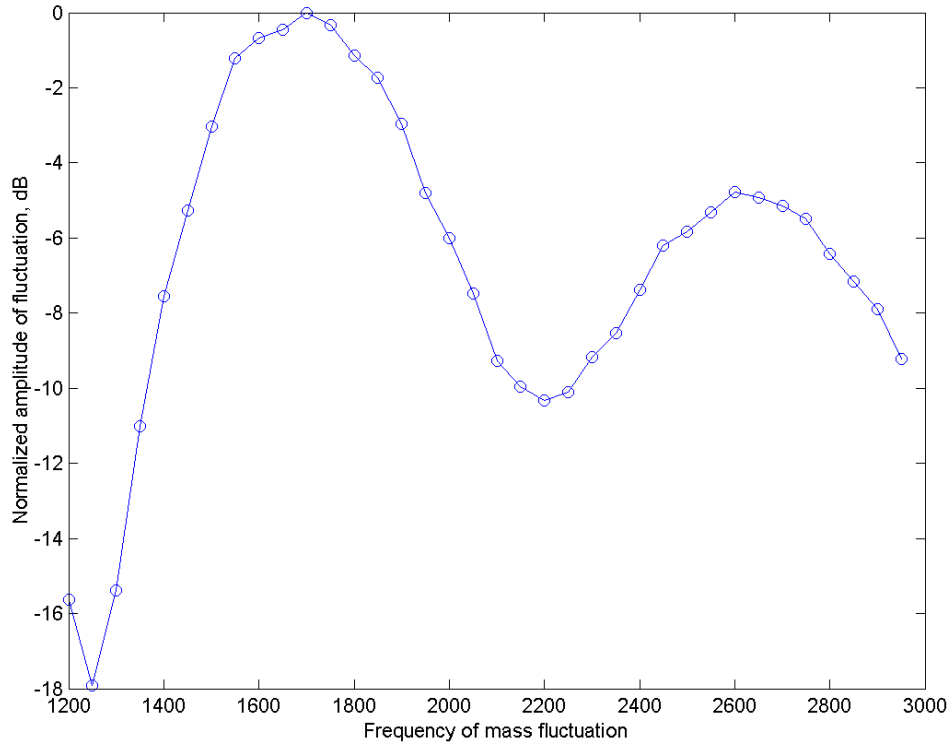

Figure 3.3: Example plot of frequency content in illumination of image case 7.

After the frequency content was found for a single instantaneous image, the process was repeated for one image from each image pair in order to obtain a more statistically valid. The information from the images was then averaged together to establish the frequency content for that particular experimental condition. The instantaneous information was combined using the relationship below.

$$P_i = \sum_k \frac{P_i^k}{\sum_i P_i^k}$$

where P_i is the power at frequency i for all of the images and k is the index to indicate the instantaneous images.

With the frequency information from the instantaneous images combined into a time-average statistically significant measurement, identification of the dominant fluctuating frequency and comparison between cases is possible. For this study only cases 2 and 7 will be compared because this analysis requires a laser intensity high enough to illuminate not only the large clumps, but also the smaller droplets. Figure 3.4 shows the frequency content of the intensity maps for cases 2 and 7.

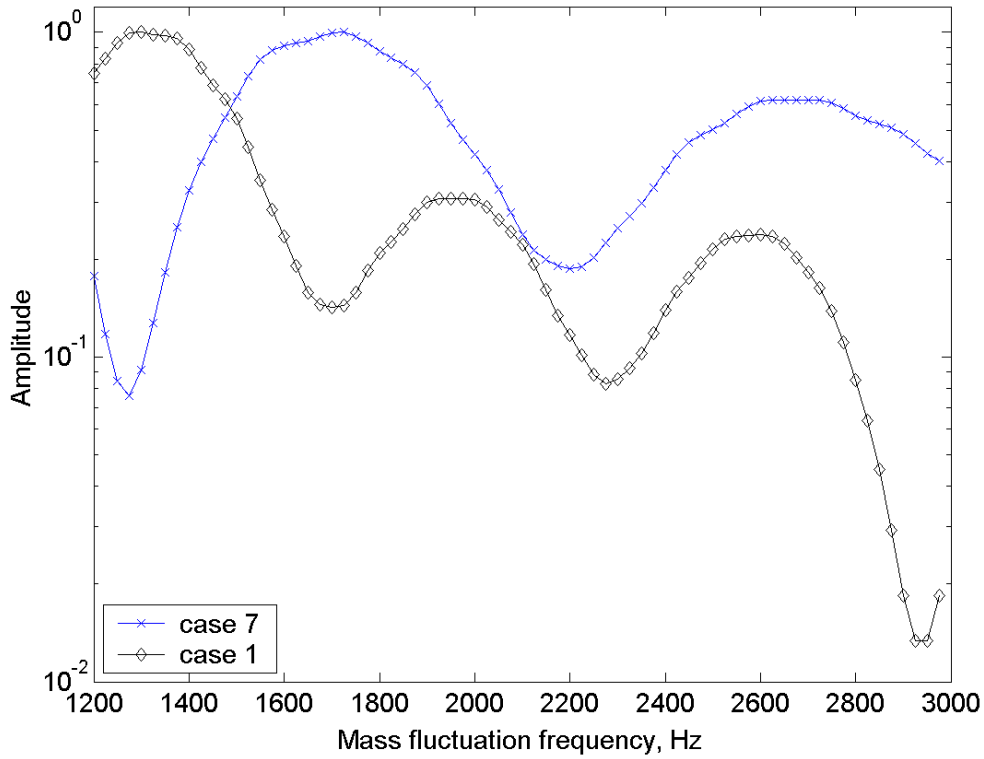

Figure 3.4: Frequency content of intensity maps for cases 2, 7, and 8

As shown in Figure 3.4 there is significant mass fluctuations at frequencies between 1 kHz and 2 kHz. Case 2 and 7 have clear peaks in the frequency response plots. The peak frequencies at 1300 Hz for case 2 and 1725 Hz for case 7 are indicative of the first unstable mode of the liquid column.

Chapter 4 Spatio-Temporal Velocity and Spray Characteristics

The analysis of spray using the instantaneous velocity field includes four major components. First, a description of the velocity field and how it changes over the varying experimental conditions is presented. Following the velocity field description, spray characteristics measurements for a representative sample of instantaeous images are outlined. Third is an outline of the time-average behavior of the spray characteristics. Finally, an examination of how the spray is effected by the predominant flow descriptors; gas phase Reynolds number, aerodynamic Weber number, Ohgnesorge number, and momentum ratio is reported.

4.1 Instantaneous Liquid-phase Velocity Field

The instantaneous velocity field of a jet in crossflow shows the general trends that are present in the time-average velocity field. Plus, the instantaneous velocity field illustrates local discontinuities from individual liquid particles, abrupt changes within the spray, a sharp gradient at the spray boundary, and fluctuating components of location for the spray characteristics. Below is an analysis of the experimental cases broken up by general characteristics and modes of liquid column breakup.

4.1.1 Cases 1 and 2: Water Jet at Ambient Temperature

The first case described is a water jet with a momentum ratio of 12 issuing out of an orifice with a diameter of 0.762 mm. The cross flow is air traveling with a velocity of 75 $^{m}/_{s}$. show an example of the instantaneous velocity field for this case compared to the averaged velocity field.

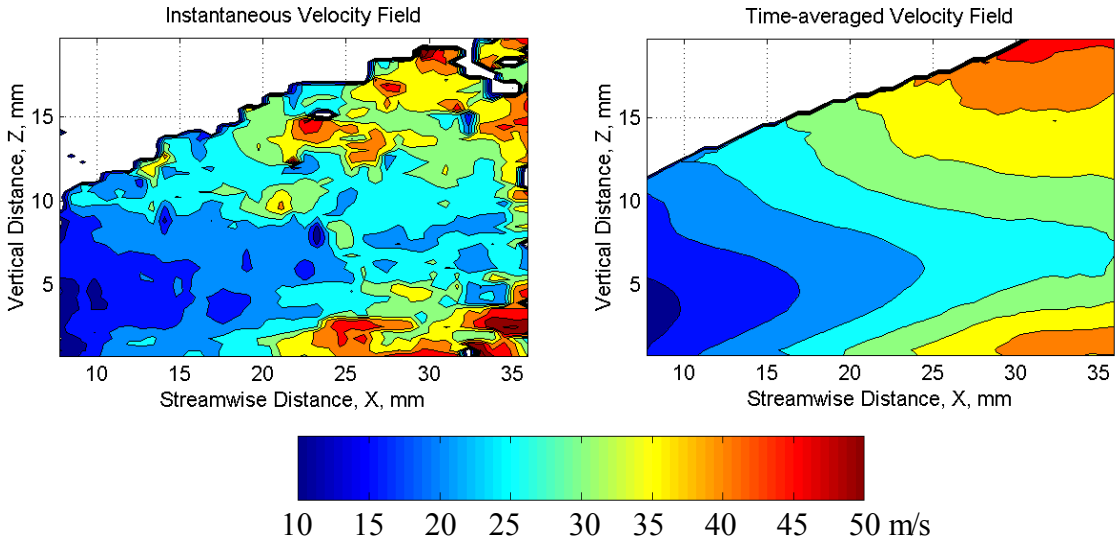

Figure 4.1: Instantaneous and time-averaged velocity fields for case 1

As shown in , the time-averaged trends of velocity gradient and spray boundary are similar, but the instantaneous images show three key differences. The first difference is the spray boundary. The instantaneous image shows an abrupt boundary between the liquid phase and the free stream gas phase. Also, the spray boundary in the instantaneous image fluctuates around a steadily growing trend while in the time-averaged image this shows up at a velocity gradient at the spray boundary. Third, the core position, designated by the minimum velocity in the instantaneous image, also fluctuates while the time-averaged velocity field shows this trend as a steady core position with smooth velocity gradients on either side. Similar trends in case 2 are illustrated in Figure 4.2.

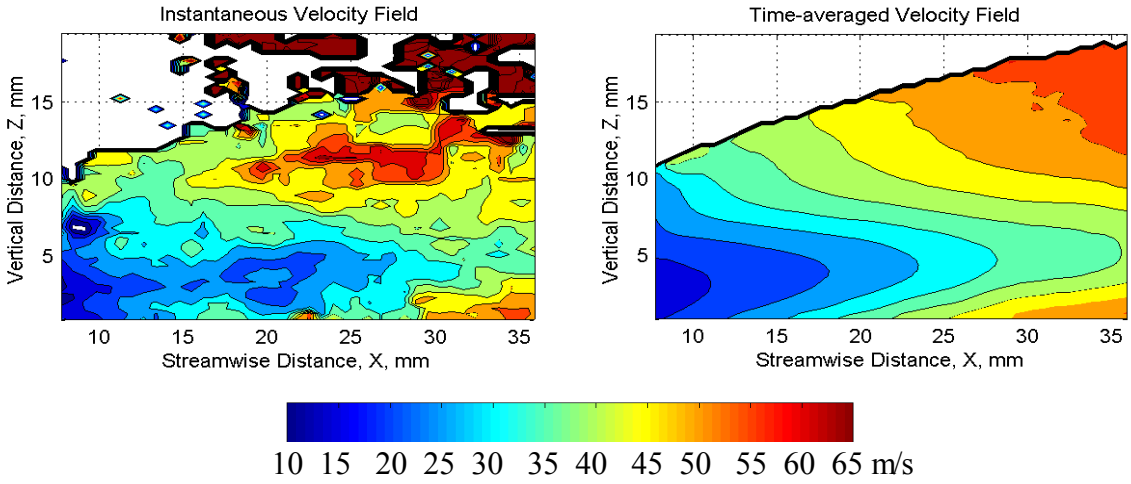

Figure 4.2: Instantaneous and time-averaged velocity fields for case 2

Both case show a well defined jet boundary and core location for the time-averaged and instantaneous cases. In addition, although cases 1 and 2 are similar for velocity distribution and spray structure, the higher aerodynamic Weber number, 165 versus 92, for case 2 forces the penetration of the liquid jet down and forces the droplets to accelerate quicker yielding a higher over all liquid velocity for this case.

4.1.2 Cases 7 and 8: Kerosene in Heated Crossflow

The second set of cases are both kerosene issuing out of the orifice at momentum ratios of 12 and 18 with a crossflow heated to a temperature 755 K. For these cases, although the aerodynamic Weber number falls in between the Weber number and Reynolds number for the previous two cases, the difference in Ohnesorge number causes the momentum exchange between the air and liquid to occur much quicker yielding shorter overall spray core. Figure 4.17 illustrates the change in spray character for case 7 compared to case 1.

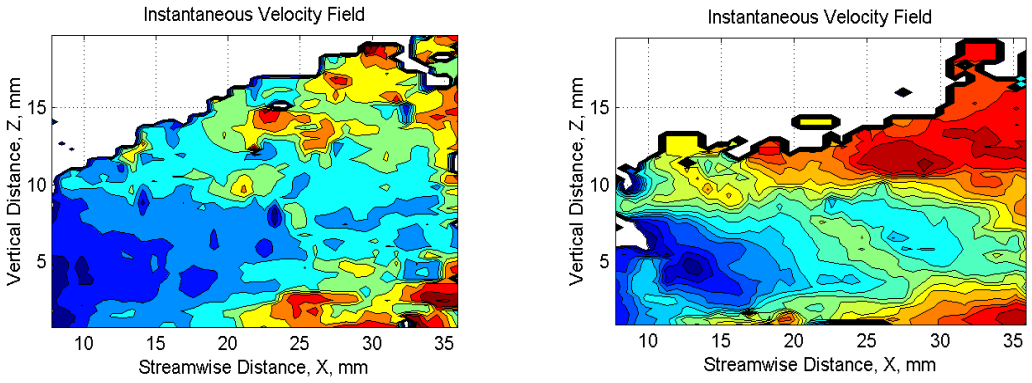

Figure 4.3: Comparison of instantaneous velocity fields for cases 1 and 7

As with the previous group of cases, Figure 4.4 and Figure 4.5 illustrate how both case 7 and case 8 have similar spray shape and velocity distributions. Also the relationship between the instantaneous and average velocity field is similar to that of cases 1 and 2. The velocity gradients near the spray boundary and bordering the spray core correlate to abrupt changes in the instantaneous velocity field juast as in cases 1 and 2.

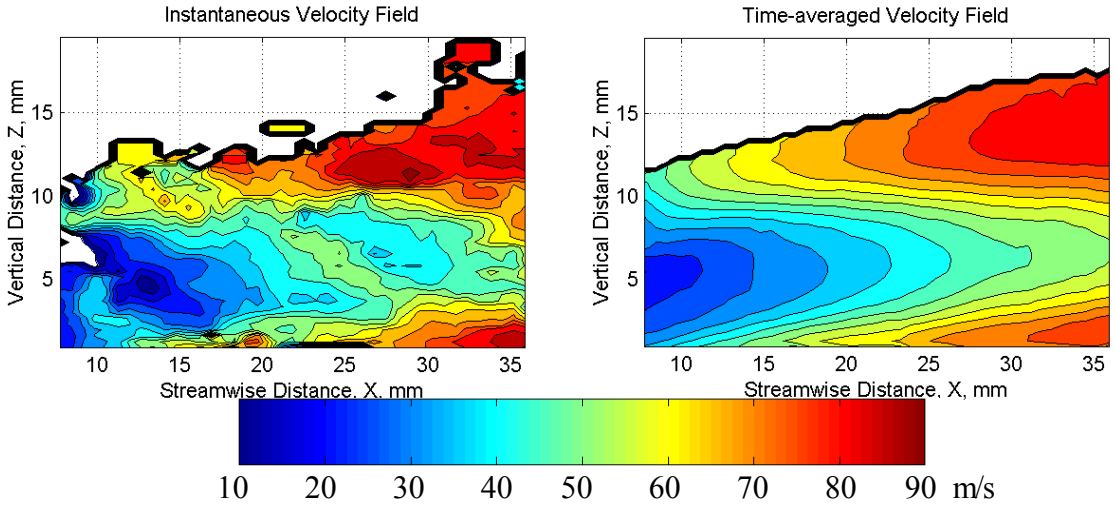

Figure 4.4: Instantaneous and average velocity fields for case 7.

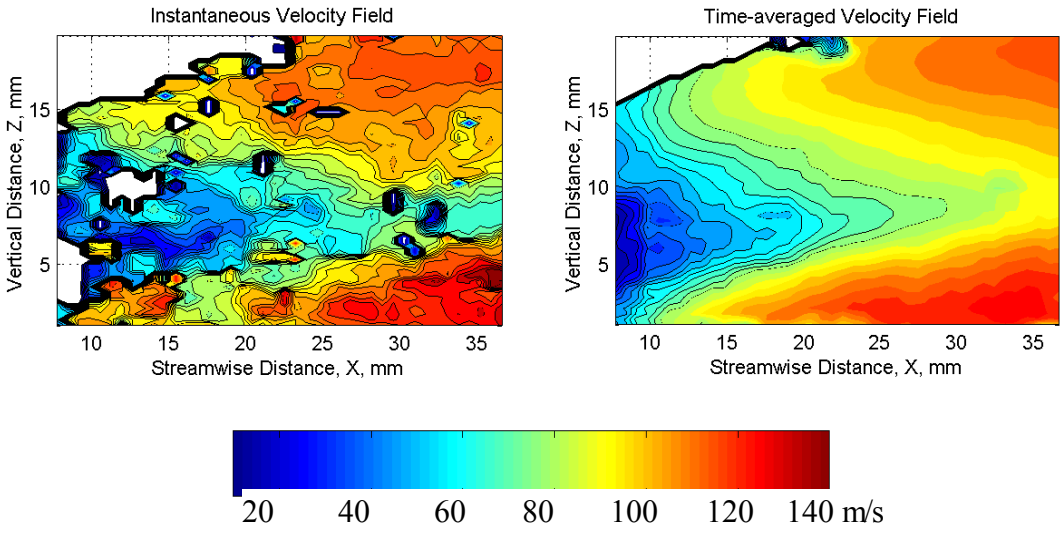

Figure 4.5: Instantaneous and average velocity field for case 8.

An additional phenomenon that is most easily identifiable with these two cases, is as the momentum ratio increases the lower boundary of the liquid spray becomes detached from the wall and an area without a significant percentage of liquid in it begins to form below the jet contributing to a shorter dissolution of an identifiable spray core. Also, this area pushes the remaining core higher giving the trajectory near the transition from near field to far field a different shape.

4.1.3 Cases 3, 4, 5, and 6: Water at High Weber Numbers and Low Reynolds Numbers

For the following cases, the combination of flow parameters resulted in spray behavior where the penetration reached a height that was outside the interrogation area investigated and the momentum exchange was such that the liquid phase still had a large vertical component causing the quantification of spray parameters to be prohibitive for these cases. Although quantitative classification is not possible in this regime of operation, the qualitative character of the spray still offers information about how the spray behaves through the range of experimental cases test.

Case 3 was composed of a water jet issuing from the orifice at a momentum ratio of 12 with a cross flow heated to 394 ^{o}C, traveling at a velocity of 137 $^{m}/_{s}$. Figure 4.6 illustrates the difference from the previous cases. In this case, and similarly in case 4, the spray core is located near to the spray boundary. For these cases the liquid column is going through a different mode of breakup. This is evidenced by the change from a spray core located in the center surrounded by higher velocity regions to the largest droplets and therefore the lowest velocities are located near the top of the jet. The change in distribution suggest that the liquid column is breaking sooner and therefore the droplets are inheriting a significant vertical velocity component which is creating the shape of the new distribution. Because of this change in the character of jet breakup, the established definition of spray core is not valid.

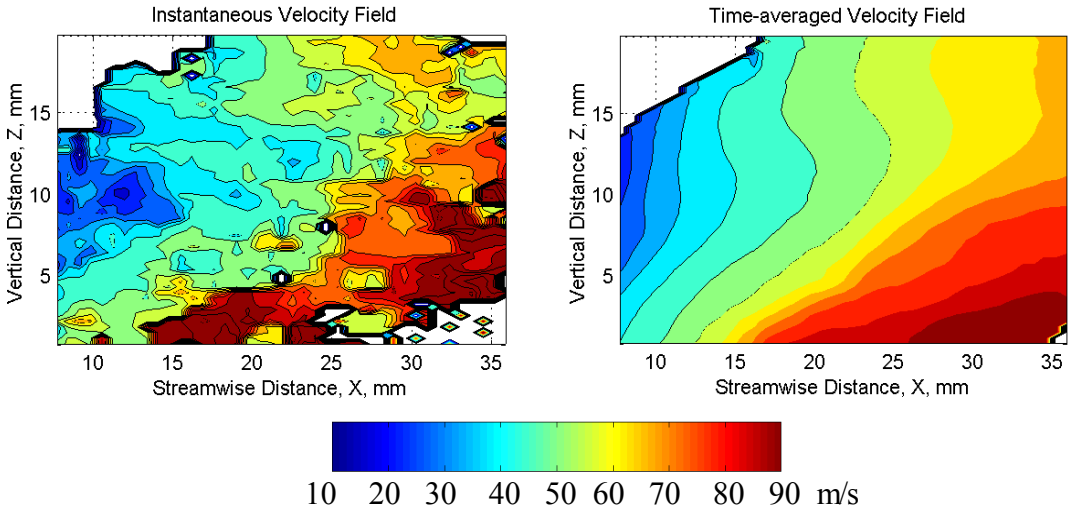

Figure 4.6: Instantaneous and time-averaged velocity field for case 4.

Further evidence for a change in the breakup mode of the liquid column is demonstrated by the instantaneous images of the liquid column. Figure 4.7 shows how the liquid column break up into droplets before it has completely turned to the direction of the air flow. The results is a droplet distribution that is skewed vertically by the momentum exchange between the gas flow to the droplets instead of a spray core centered in the spray with an even distribution of droplets surrounding it.

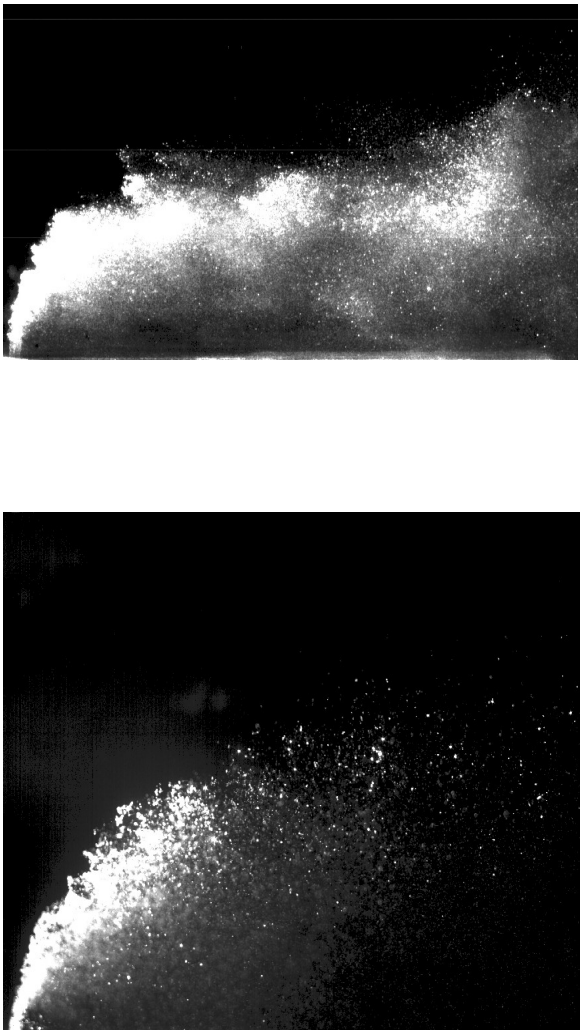

Figure 4.7: Instantaneous images of the liquid column for cases 3 (bottom) and 7 (top).

Cases 5 and 6 show a further transition from the momentum exchange happening predominantly while in the liquid column to momentum exchange occurring while the liquid is in droplet form. Figure 4.8 illustrates how for cases 5 and 6 only the smallest

droplets, with velocities near the free stream, complete the acceleration from vertical to horizontal velocity direction within the interrogation region.

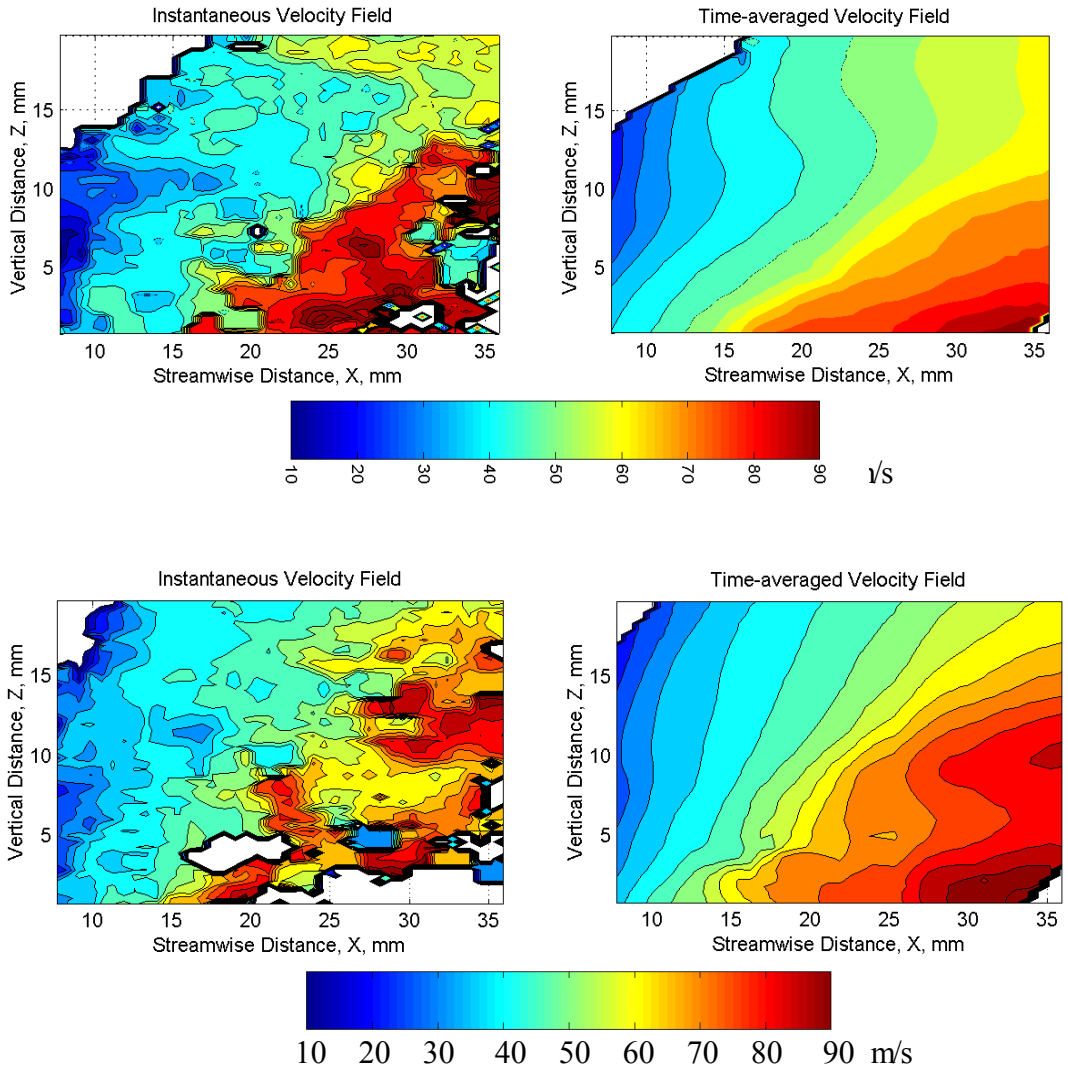

Figure 4.8: Instantaneous and average velocity field for case 5 (top) and case 6 (bottom).

Because of the difference in character of case 3, 4, 5, and 6 these cases will be excluded in the discussion of spray penetration and core trajectory in the following sections.

4.2 Spray Penetration and Core trajectory

The penetration for the data collected all show good agreement with the behavior established by studies spanning three decades when analyzed using the averaged velocity field for location of the desired characteristics. When the instantaneous images are analyzed, however, two major differences from the currently established studies become apparent. First, the time-averaged penetration arrived at when first analyzing the instantaneous images and then averaging these values together is lower then the penetration established using the time-averaged velocity field. Second, there is a fluctuating component to the penetration that is not accounted for in the time-averaged measurement. The behavior of the core also shows definite trends that are similar from case to case and show correlations to the time-averaged data.

4.2.1 Instantaneous Spray Penetration and Core Trajectory

As described in the experimental procedure, the spray penetration was designated as the highest point in the velocity field grid that contained a velocity vector within the bounds of magnitude set at for each x-location in the grid. The core trajectory was correspondingly identified as the grid point with the lowest x-direction velocity inside of the spray. Figure 4.9 gives an example of one instantaneous image with the identified

penetration and core location at each x-direction grid point. The accuracy of these measurement is base on the grid size which has steps of 0.704 mm in the x-direction and 0.352 mm in the z-direction, or approximately one orifice diameter and half of a orifice respectively.

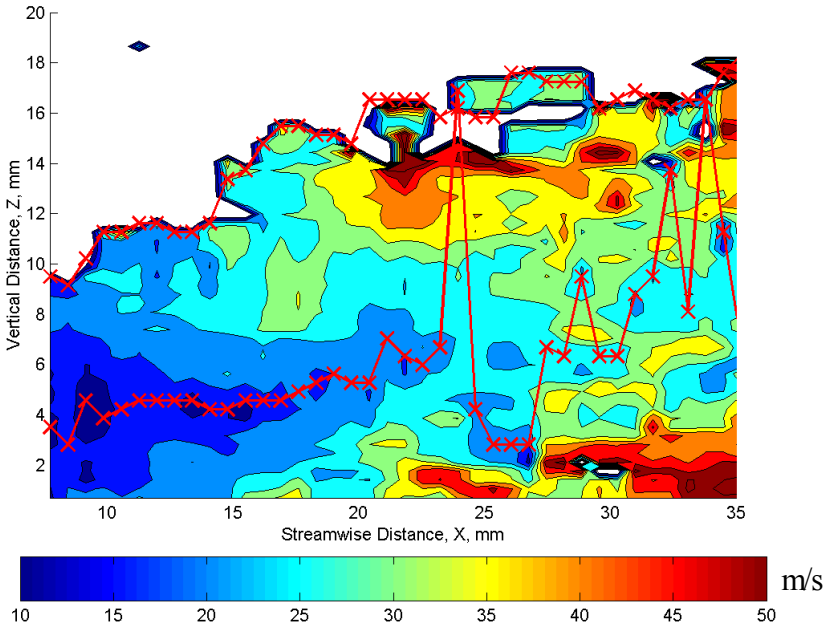

Figure 4.9: Instantaneous identification of the spray penetration and core trajectory.

As illustrated, the penetration does not always follow the boundary of the spray for several reasons. One source of error in the method of penetration identification is the method simply counts the number of grid points containing a valid velocity vector starting from the bottom of the grid, so if there is a gap in the grid then the penetration measurement will yield a value slightly lower then the real measured value. In addition, the spray boundary is not a continuous single valued function of streamwise distance, x,

so when the physical spray boundary folds back on itself, the measured penetration is the average value of both penetrations. Since each point in the penetration is averaged with 1500 independent measurements in time, these two errors become outliers and do not contribute significantly to the final results of the penetration measurement. A third contribution to the appearance of discrepancy between the penetration located by the line and the spray boundary designated by the contour plot is the interpolation completed by the plotting program and has no effect on the relationship of the measured results to physical reality.

The core location, as represented in Figure 4.9, also shows some discrepancy to what visually appears to be the core of the spray. The errors to these measurements must be broken up into two categories. The first category is those error cause by large droplets or noise sources in the digital image that yield a velocity much lower then the surrounding velocities and therefore yield a core location that is not representative of the mass flux profile. As with the penetration, these errors occur randomly and therefore will become outliers when analyzed with the other instantaneous images. In the rare case where the noise effects all or a large number of the images, it is identified and excluded on a case by case basis. The second category of error in the core measurements occurs as the spray transitions from the near field to the far field. Part of the change in spray character at the transition is the dissolution of the spray core. Although the core location appears random in the instantaneous images, on a time-averaged basis there is still a stable mean and fluctuating component. The difference is that the distribution in this

area is truly dependent on the random probability of the breakup process for individual droplets as opposed to a more deterministic, but fluctuating process occurring upstream.

4.2.2 Overview of Individual Cases

For case 1, Figure 4.10 shows the instantaneous velocity field plus both the penetration and core trajectory demarcated by red X's connected by a red line. In this case, the core breaks at 23 mm as indicated by the change in character of the contour lines from concentric to broken and scattered and at this point the core trajectory fluctuates at a much larger amplitude than upstream of this point.

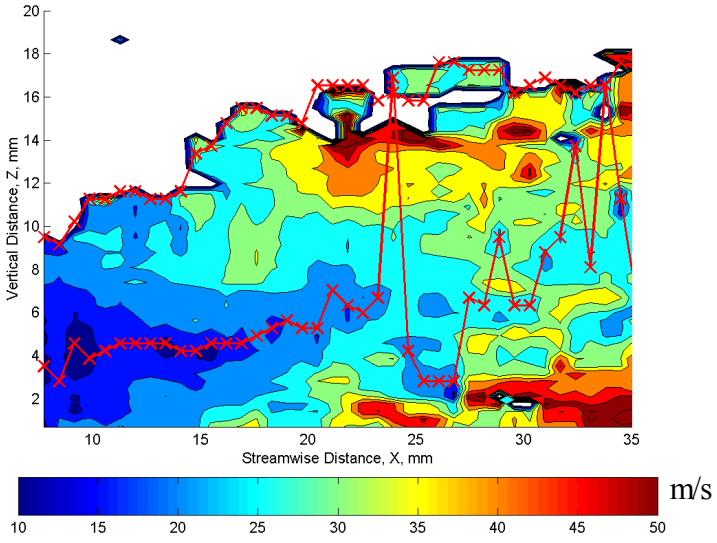

Figure 4.10: Instantaneous velocity field, spray penetration, and core trajectory for case 1.

The fluctuation in the spray penetration is obvious in Figure 4.10, showing a smooth trend of increasing height similar to the shape proposed by numerous researchers (Inamura and Nagai, 1997) but in addition to this trend is a fluctuating component that is also present. The same trends are illustrated for cases 2 and 7, as shown below in Figure 4.11 and Figure 4.12.

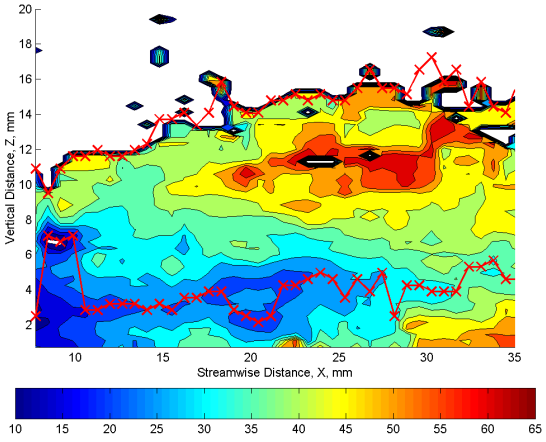

Figure 4.11: Instantaneous velocity, penetration and core location for case 2.

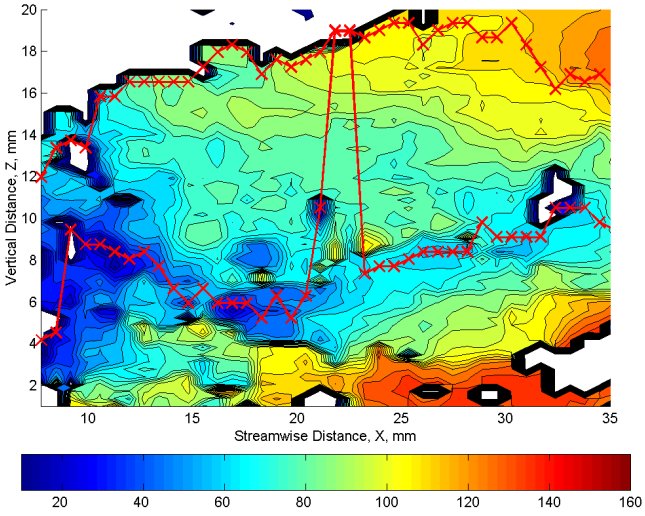

Figure 4.12: Instantaneous velocity, penetration, and core trajectory for case 8.

For case 7, comparison of the penetration and core location overlaid on an instantaneous velocity field and an the instantaneous image that was used to produce the velocity field shows good agreement between the raw image, the velocity field, and the measurement of the penetration and core location.

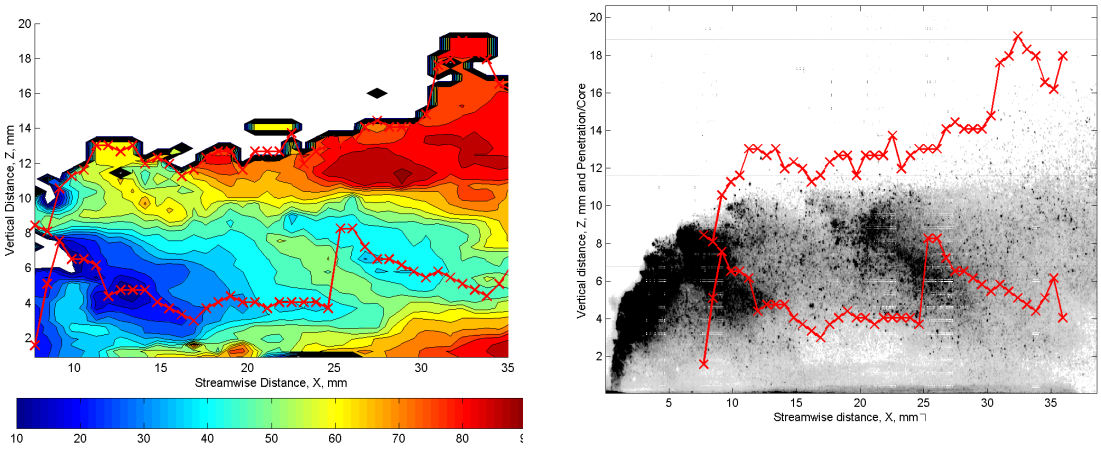

Figure 4.13: Instantaneous velocity, penetration and core location for case 7.

The next step in processing the raw data to reveal spray characteristics was to average the instantaneous measurements from each image to yield an average and distribution. The following chapter details the time average results.

4.2.3 Time-averaged Results from Instantaneous Analysis

After each instantaneous image had been processed, then the mean and standard deviation were taken at each x-location. The mean was calculated and the amplitude was express as a percent of the mean value.

Just as the velocity fields becomes continuous and smooth when average over time, so do the spray penetration and core trajectory. Figure 4.14 shows the average velocity field with the average penetration and core location plotted. The error bars represent one standard deviation from the mean. Here, the standard deviation represents the root mean squared amplitude of fluctuation.

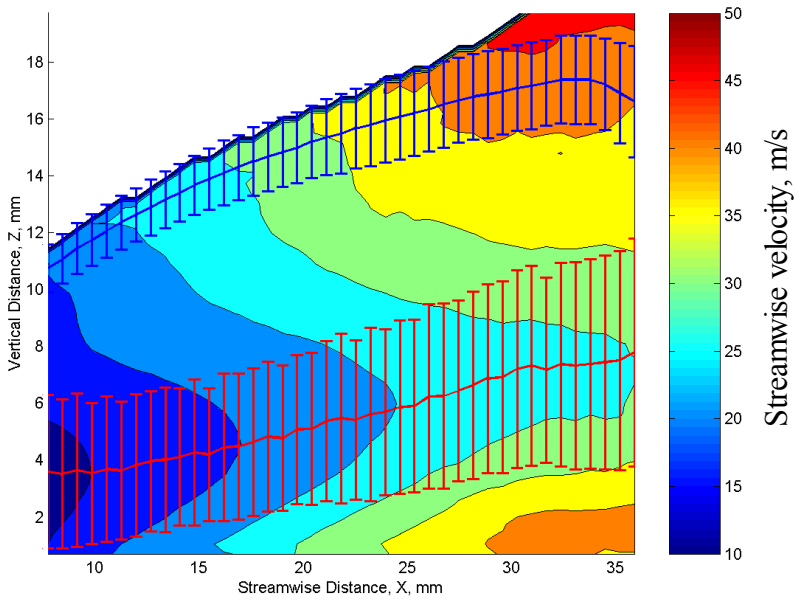

Figure 4.14: Time-averaged velocity profile, spray penetration and core location for case 1.

Overlaying the average and standard deviation of the jet characteristics points out relationships between the instantaneous behavior of the spray and characteristics of the time-averaged velocity field. The first relationship is that the mean values for penetration and and core location both line up with local minimuma in the average velocity field. Second the values of the standard deviation, or root mean squared amplitude line up with changes in inflection of the contours of velocity. These two relationships point out that the average velocity field is more an illustration of the fluctuating characteristics of the spray and the statistical distribution of these characteristics then solely a map of the steady state behavior. The values from case 2 and case 7 demonstrate the same relationships that occur in case 1, as shown in Figure 4.15 and Figure 4.16.

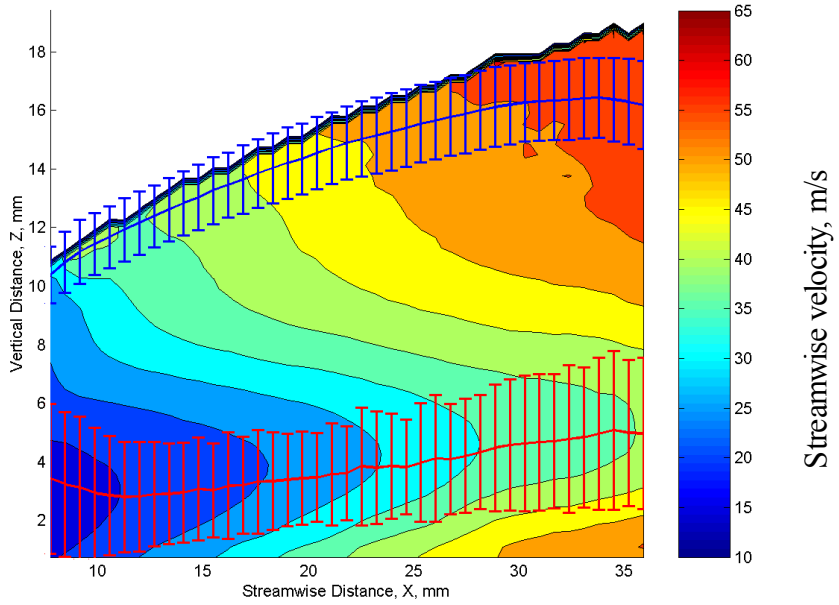

Figure 4.15: Time-averaged velocity field, spray penetration and core location for case 2.

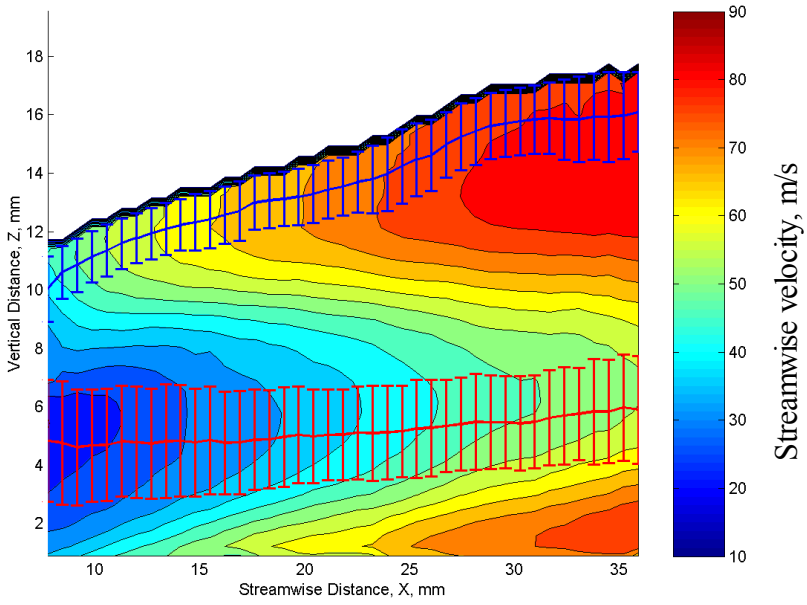

Figure 4.16: Time-averaged velocity field, spray penetration and core location for case 7.

Cases 1, 2, and 7, show similar trends with a well defined spray core and a velocity gradient near the spray boundary. Also, similar penetrations occur for all three case which agrees with Chen's suggestion that penetration is only a function of momentum ratio and streamwise distance. (Chen, Smith and Schommer, 1993)

Case 8, shown in Figure 4.1, demonstrates the effects of changing the momentum ratio from 12 to 18. The air flow and aerodynamic Weber number are the same for case 8 as they are for case 7. By changing only the momentum ratio, the core height changes, the bottom of the spray has detached from the vane, the penetration has increased in both absolute value and fluctuation growth rate, and the core accelerates much quicker then in any of the previous cases. Although, the jet is different in many ways, the droplet distribution is the same. Also, there is still a well defined core of lowest velocity with increasing velocity surrounding it and a velocity gradient near the spray boundary , demonstrating that this case still has the same mode of liquid column breakup and therefore can be included in the comparison of spray penetrations and core trajectories.

Some limitations for this case will need to be made because of the limitations of the interrogation coverage of the spray and the noise effecting measurements near a streamwise distance of 22 mm near the top of the jet. To accommodate these two issues, the penetration values after 20 mm and the core values between 20 and 25 will be excluded from the comparison of spray characteristics.

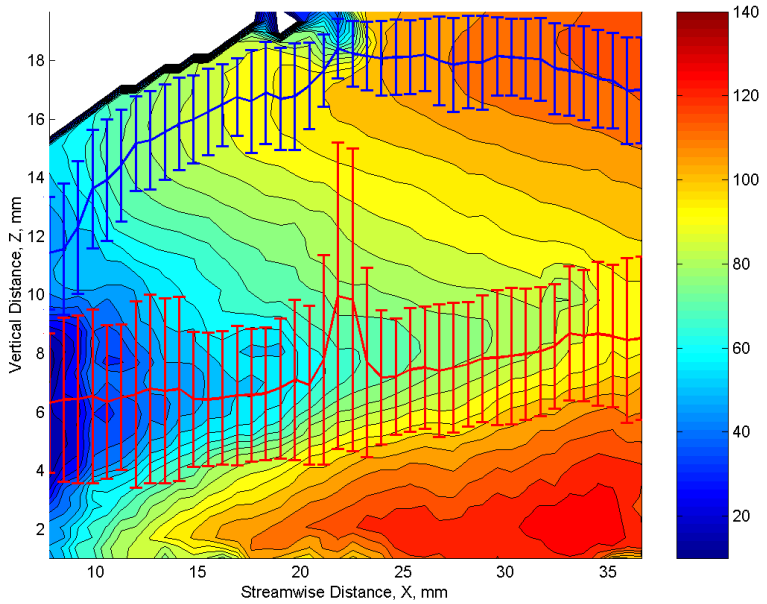

Figure 4.17: Time-averaged velocity, spray penetration and core location for case 8.

4.2.4 Case Comparison

Figure 4.18 shows a comparison of the penetration heights and core location for cases 1, 2, 7 and 8. For all three cases with a momentum ratio of 12, cases 1, 2, and 7, the trend of penetration agree with Chen suggestion of how penetration grows with streamwise distance. In addition, the penetration heights for these three cases are also similar over changes in air velocity, air temperature, Ohnesorge number, and Weber

number which further supports the conclusion that penetration height is only a function of momentum ratio.

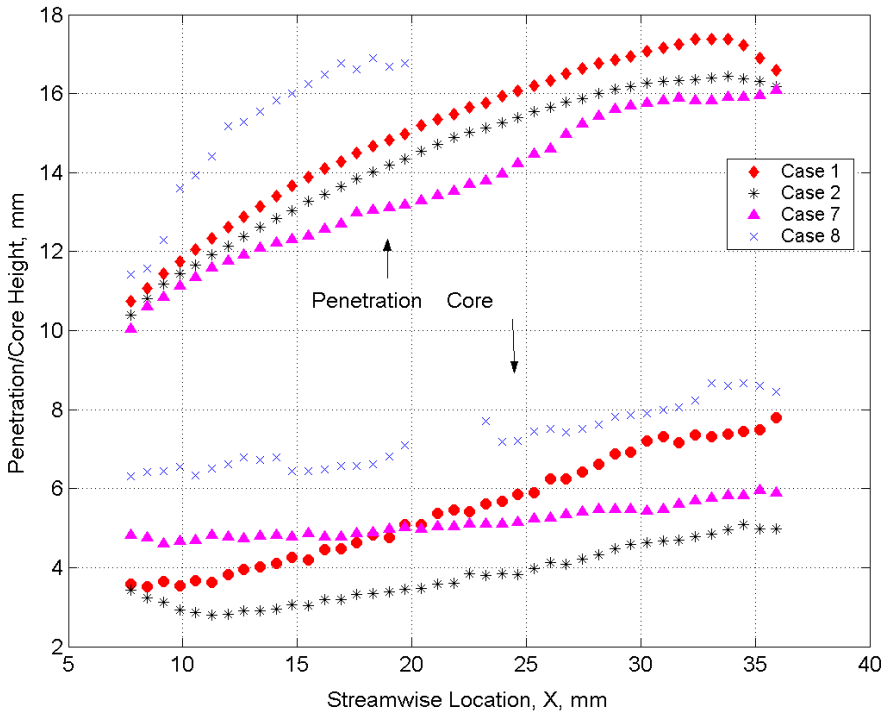

Figure 4.18: Comparison of penetration and core location.

Core location on the other hand appears to be dependent on many factors. The trend of the core location changes between the first two cases and the last two case suggesting a dependence on Ohnesorge number, while the amplitude of the core height changes with changes in both momentum ratio and air velocity.

In addition to comparison of the time-averaged values of spray penetration and core location, which have already been established by previous studies, the fluctuation

amplitudes of these values also needs to be correlated to the flow parameters. Figure 4.19 shows a plot of the root mean squared, RMS, amplitudes of fluctuation for the spray penetration and core location.

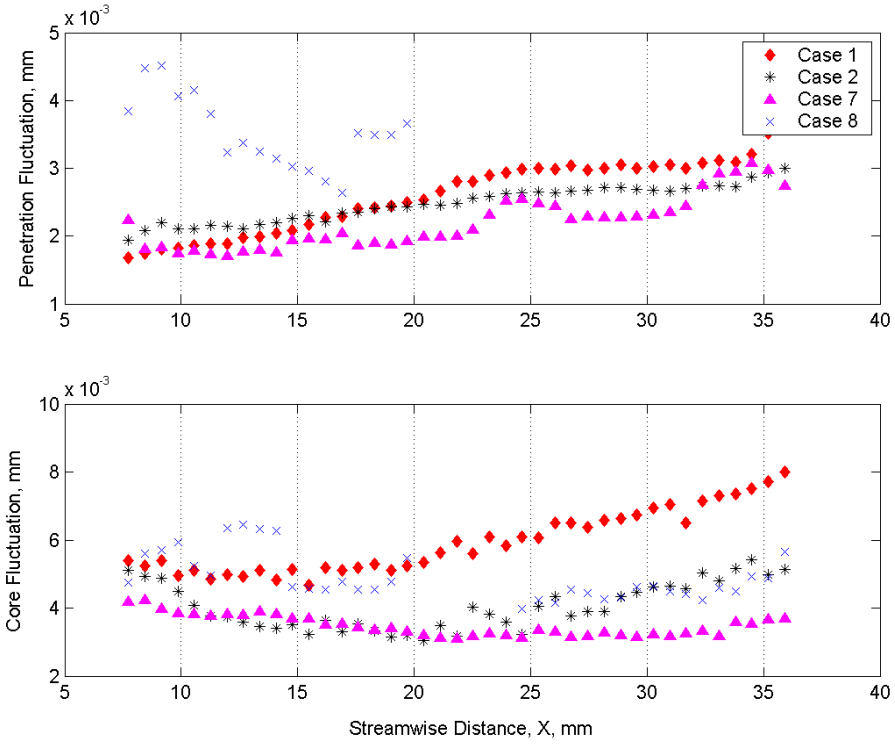

Figure 4.19: Comparison of fluctuation amplitude for penetration and core height.

Similar to the penetration height, the fluctuation amplitude appears to only be dependent on the momentum ratio. Case 8 is the only case to show a significant difference in amplitude of fluctuation and is the only case that was not run at a momentum ratio of 12. For cases 1, 2, and 7 the fluctuation of the penetration is stays near 20% of the total amplitudes and for core location the fluctuation is between 30 and 50% of the amplitude. The core location also has only one case that differs in trend.

Case 1 the case showing an increase in fluctuation amplitude with increasing streamwise distance, is the case with the lowest Weber number suggesting the dominant factor for core fluctuations in the spray.

Chapter 5 Conclusions and Future Work

A liquid jet in a crossflow is composed of three segments, each with their own characteristics. With the TRDPIV system, the holistic properties of all three segments of a jet in crossflow were acquired with a single measurement. This allowed for comparison of system characteristics across not only individual pieces of one segment of the jet, for example PDA measurements of many droplets in one point of the far field spray, but characteristics across the entire system including the liquid column, near field spray, and far field spray simultaneously in a fashion that allowed for direct comparison between the different segments.

Although current technology and studies demonstrate that holistic measurements across multiple segments of a liquid jet in a crossflow are possible, much work still needs to be done to further the knowledge of the governing forces dictating the behavior of these segments, and how individual particles affect each other when in close proximity.

Knowledge about mass fluctuations and spray characteristics fluctuations gained in the current study can be increased with further study with a liquid jet in crossflow.

5.1 Mass Fluctuations

The instantaneous images recorded demonstrate that the is certainly a fluctuation in the streamwise direction of the total mass in the spray. The results also point out that these fluctuations are in the frequency range of 1 kHz to 2 kHz, which are in a similar range to those reported by previous studies.

Incorporating the mass fluctuations in combustor modeling and design efforts will allow for better prediction of unsteady phenomena in the flame frond an downstream flow field. Also, understanding of the drivers of time-averaged spatial distributions in droplet size and velocity can be gained.

5.2 Spray Characteristics

Initially, motivation behind the study was soley to compile a database of time-averaged spray at specified operating conditions. Because of the nature of PIV, the spatio-temperal characteristics of the jet were revealed. Through analysis of these variations in space and time, three major conclusions were reached.

1) The near field and far field of the spray fluctuates in a manner similar to that found on the liquid column in a jet in a crossflow experiment.
2) These fluctuations are observable in the spray penetration height, the core trajectory, and the cross-sectionally averaged mass flux.
3) These variations effect time-average measurements in such a manner that the time varying components are revealed through spatial gradients in the averaged information.

5.3 Recommendations for Future Work

During processing and analyzing the data from the current study, many limitations and obstacles were revealed that were not apparent initially. Also, due to the large

physical scale of the setup and the long time scale require to reduce PIV data, additional experiments to repeat data sets or complete a more inclusive matirx of experimental conditions would require significant time and effort. Below are some suggestions for how to best complete the data set to better elucidate the measurements and trends pointed out in this study.

1) A more inclusive data set including a range of momentum ratios, gas phase Reynolds numbers, aerodynamic Weber numbers, and Ohnesorge numbers beginning at a momentum ratio of 18 and working down would be beneficial. With a more inclusive data set, many of the trends and correlations pointed out in the current study could be quantified. Also, by staying below a momentum ratio of 18, the spray height will stay within the limitations of the interrogation area.
2) Data was collected using a time resolved DPIV system, but the sampling frequencies were too low to resolve the fluctuation frequencies of the spray in time. Future experiments acquired with a sampling frequency configured to resolve the frequencies in time would allow the study and comparison of the frequencies found in space and time. In addition to having to simultaneous measurements of the same phenomenon, the comparison of the frequencies found in space and time could reveal information about the acceleration of droplets within the spray

3) Some of the limitations from data processing occur because a single image contained both the liquid column and the spray. This could be resolved by using two phase locked cameras and one laser sheet. With this method the measurement of both the liquid column and the spray regions could be independently optimized while retaining the phase locking that allows for spatial resolution of time dependent phenomena.

4) While droplet sizing is possible with the PIV system, a large field of view was deemed more important than a high resolution for the current set of experiments. Using the information gathered in the study, smaller regions could be selected to detail the droplets size of the regions of interest and the correlations from these areas could be used to predict the droplet sizes in other regions of the jet

5) A complete air only velocity field including boundary layer height, without the spray should be conducted in order to completely characterize the air flow and to compare the current experimental data with studies conducted at other facilities.

Bibliography

Aalburg C, van Leer, Faeth GM, *Deformation and Drag Properties of Round Drops Subjected to Shock-wave Disturbances*, AIAA Journal **41**: 12, pp 2371-2378, 2003

Abiven C and Vlachos PP, *Super Spatio-temporal Resolution, Digital PIV System for Multi-phase Flows with Phase Differentiation and Simultaneous Shape and Size Quantification*, Proceedings of ASME IMECE, 2002

Adrian RJ, *Particle-imaging Techniques for Experimental Fluid Mechanics*, Annual Review of Fluid Mechanics, **23**, pp261-304, 1991

Bachalo WD and Hauser MJ, *Phase/Doppler analyses for Simultaneous Measurement of Drop Size and Velocity Distribution*, Optical Engineering, **23**: 583-590, 1984

Bate CJ, Ayob R, *Annular Two-phase Flow Measurements Using Phase Doppler Anemometry with Scattering Angles of 30^o and 70^o*, Flow Measurements and Instrumentation, **6**: 1, pp 21-28, 1995

Becker J, Hassa C, *Breakup and Atomization of a Kerosene Jet in Crossflow at Elevated Pressure*, Atomization and Spray, **11**, pp. 49-67, 2002

Chen TH, Smith CR, Schommer DG, *Multi-zone Behavior of Transverse Liquid Jet in High-speed Flow*, AIAA paper 93-0455, 1993

Chishty WA, *Effects of Thermo-acoustic Oscillations on Spray Combustion Dynamics with Implications for Lean Direct Injection Systems*, PHD Dissertation, Virginia Polytechnic Institute and State University, Jun 2005

Green SM, Nejad AS, Roe LA, *Phase Doppler Anemometry Measurements of a Liquid Jet Injected Tranversely into a Gaseous Free Stream*, AIAA 94-0556, 1994

Hilbing JH, Heister SD, *Nonlinear simulation of a High-speed, Viscous Liquid Jet*, Atomization and Spray, **8**, pp. 115-178, 1998

Inamura T, Nagai N, *Spray Characteristics of Liquid Jet Traversing SubsonicAirstreams*, Journal of Propulsion and Power, **13**: 2, pp 250-256, 1997

Inamura T, *Trajectory of a Liquid Jet Traversin Subsonic Airstreams*, Journal of Propulsion and Power, **16**: 1, pp. 155-157, 1999

Inamura T, Tsutagawa T, Seong JC, and Masuya G, *Numerical Simulation on the Behavior of a Liquid Jet into an Air Flow*, Heat Transfer – Asian research, **30**:6, pp.473 – 484, 2001

Less DM, Schetz JA, *Transient Behavior of Liquid Jets Injected Normal to a High-Velocity Gas Stream*, AIAA Journal, **24**: 12, pp 1979-1986, 1986

Less DM, *Transient Behavior of Liquid Jets Injected Normal to a High Velocity Gas Stream*, PHD Dissertation, Virginia Polytechnic Institute and State University, February 1985

Mayer WH, Branam R, *Atomization Characteristics on the Surface of a Round Liquid Jet*, Experiments in Fluids, **36**, pp 528-539, 2004

Michou Y, Pichard C, and Gokalp I, *Droplet Size Distribution and residence Time Effects on a Lean Partially Premixed Turbulent Spray Flame*, Eighth International Conference on Liquid Atomization and Spray Systems, Pasadena CA, 2000

Press WH, Teukolsky SA, Vetterling and WT Flannery BP, Numerical Recipes in Fortran: The Art of Scientific computing, 2nd edition, Cambridge University Press, pp. 569-573, 1992

Rayleigh, Lord, *On the Instability of Jets*, Proc. of London Math Soc., **X**:4, 1878

Sallam KA, Aalburg C, and Faeth GM, *Breakup of Round Nonturbulent Liquid Jets in Gaseous Crossflow*, AIAA Journal, **42**:12, pp. 2529-2540, 2004

Schetz JA, Padhye A, *Penetration and Break-up of Liquid Fueld Jets in High Subsonic Speed Air Streams*, AIAA 15th Aerospace Sciences Meeting, Los Angeles, CA, January 1977

Varga CM, Lasheras JC, Hopfinger EJ, *Initial Breakup of a Small-diameter Liquid Jet by a High-sped Gas Stream*, Journal of Fluid Mechanics, **497**, pp 405-434, 2003

Appendix A: Experimental Setup Details

Equipment	*Manufacturer*	*Model No.*
Kerosene pump	Anderson Bowen	710-1-1800
Kerosene pump motor	Worldwide Corp.	WW-1-14-31C
Kerosene rotameter	Matheson	FM-1050-VI
Kerosene pressure transducer	Omega	PX212-1KGV
Methane dryer	Air Cel Systems	AR 30/S
Methane regulators	Grove Valve	MITY MITE 94
Methane valves	Flowserve	Valtek (multiple valves)
Methane pressure transducers	Kobold	SEN-8700
Methane flow meter	Eldridge Products Inc.	XDHDGCX
Main air compressor	Kaeser	FS440
Secondary air compressor	Ingersol-Rand	SSR-EP40SE
Air dryer	Kaeser	KRD1200
Air valves	Flowserve	Valtek (multiple valves)
Air flow meter	Eldridge Products Inc.	XDHDGCX
Air pressure transducers	Kobold	SEN-8700
Air thermocouples	Omega	(multiple models)
Test section thermocouples	Omega	(multiple models)
Test section pressure transducers	Setra	2651050WD11T1F
Cooling water pump	Hydra-cell	D10XKCGSHEHA
Cooling water pump motor	Anderson Bowen	

Appendix B: Test Section Details

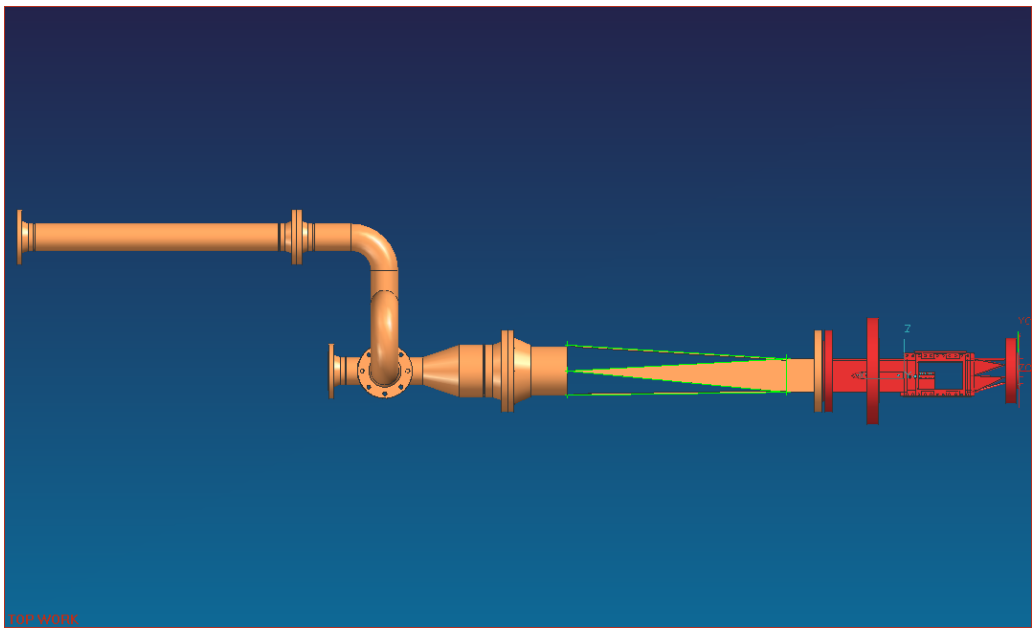

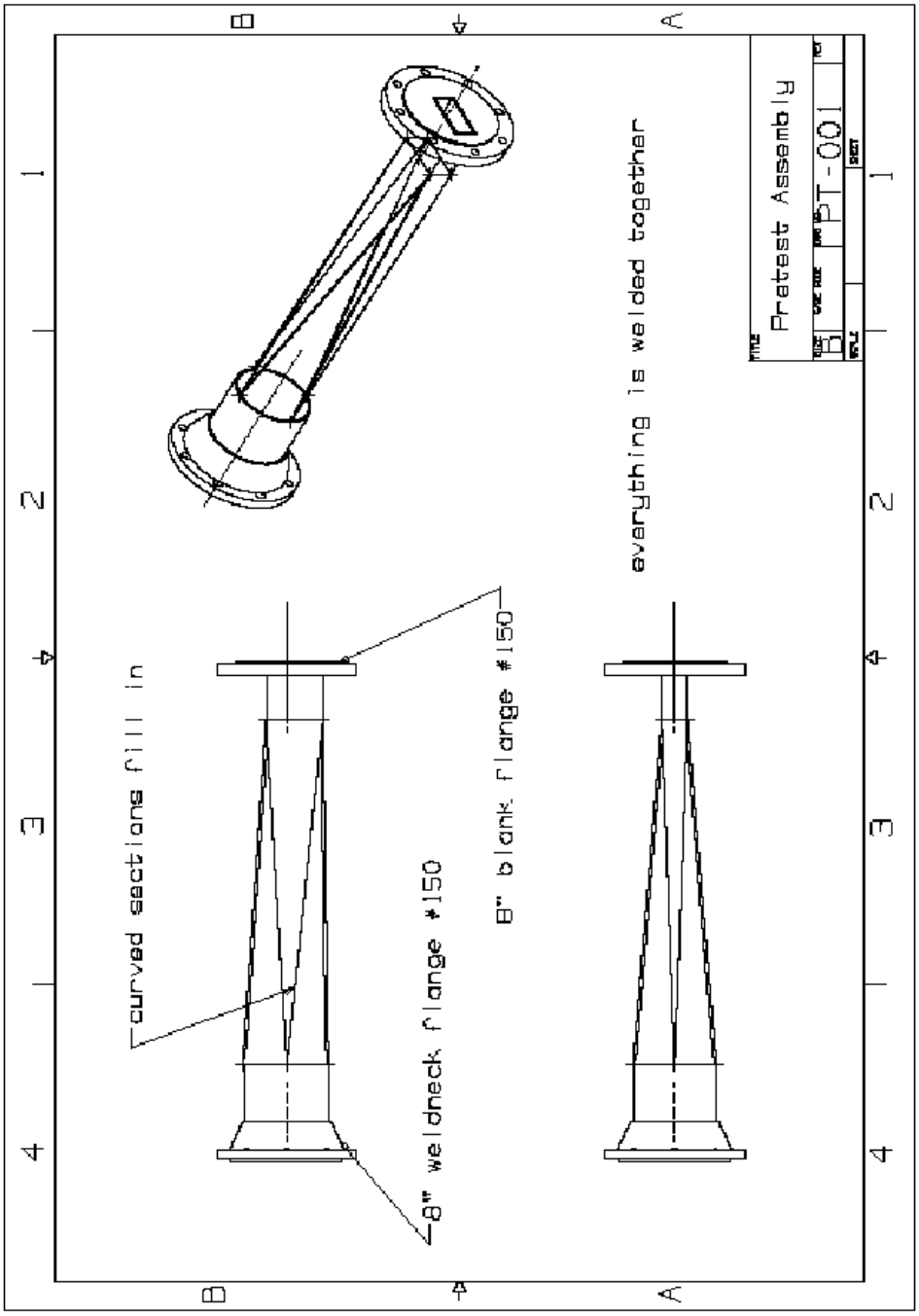
Pretest Assembly
PT-001
everything is welded together
curved sections fill in
8" blank flange #150
8" weldneck flange #150

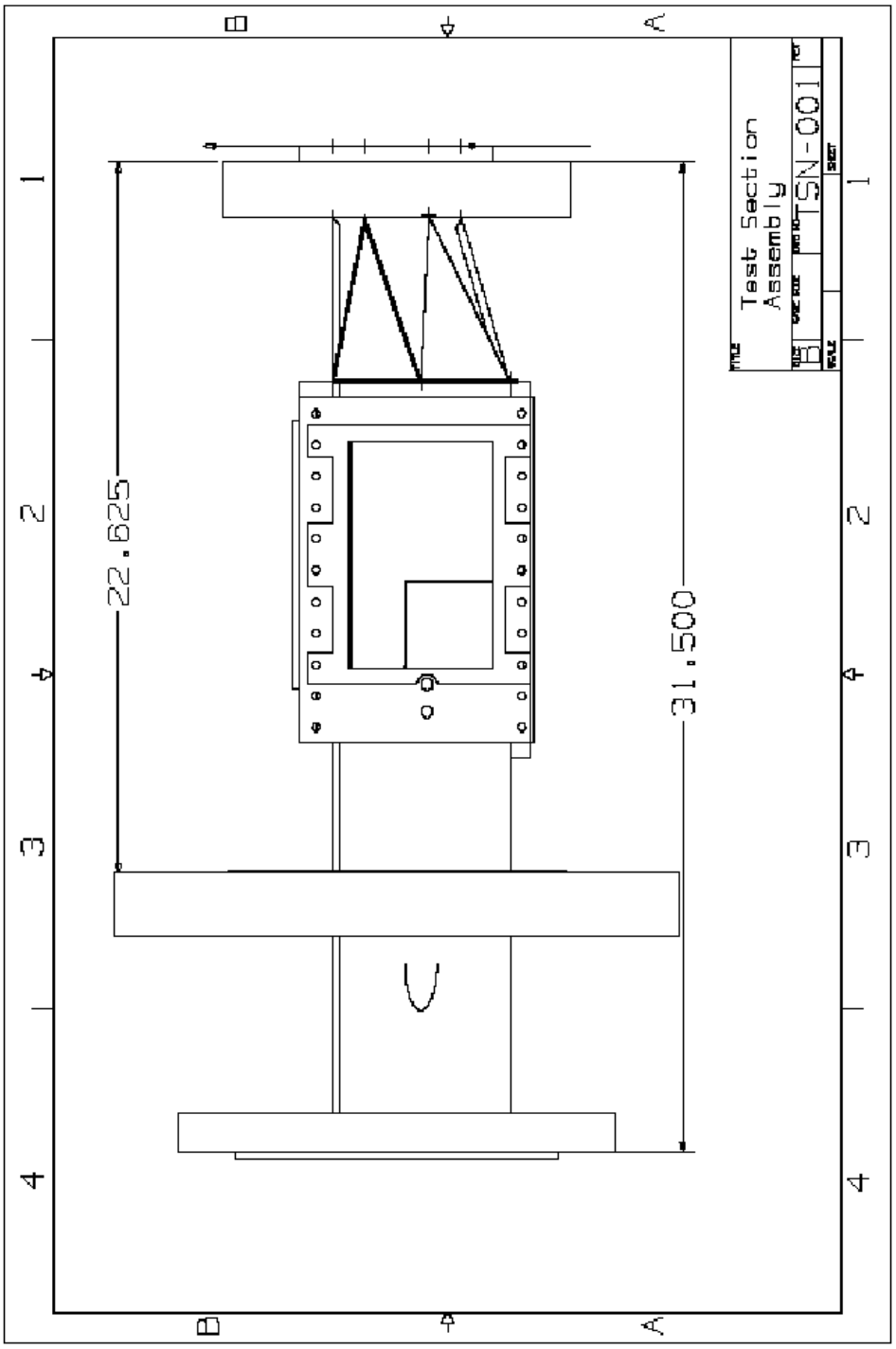
Test Section Assembly
TSN-001
22.625
31.500

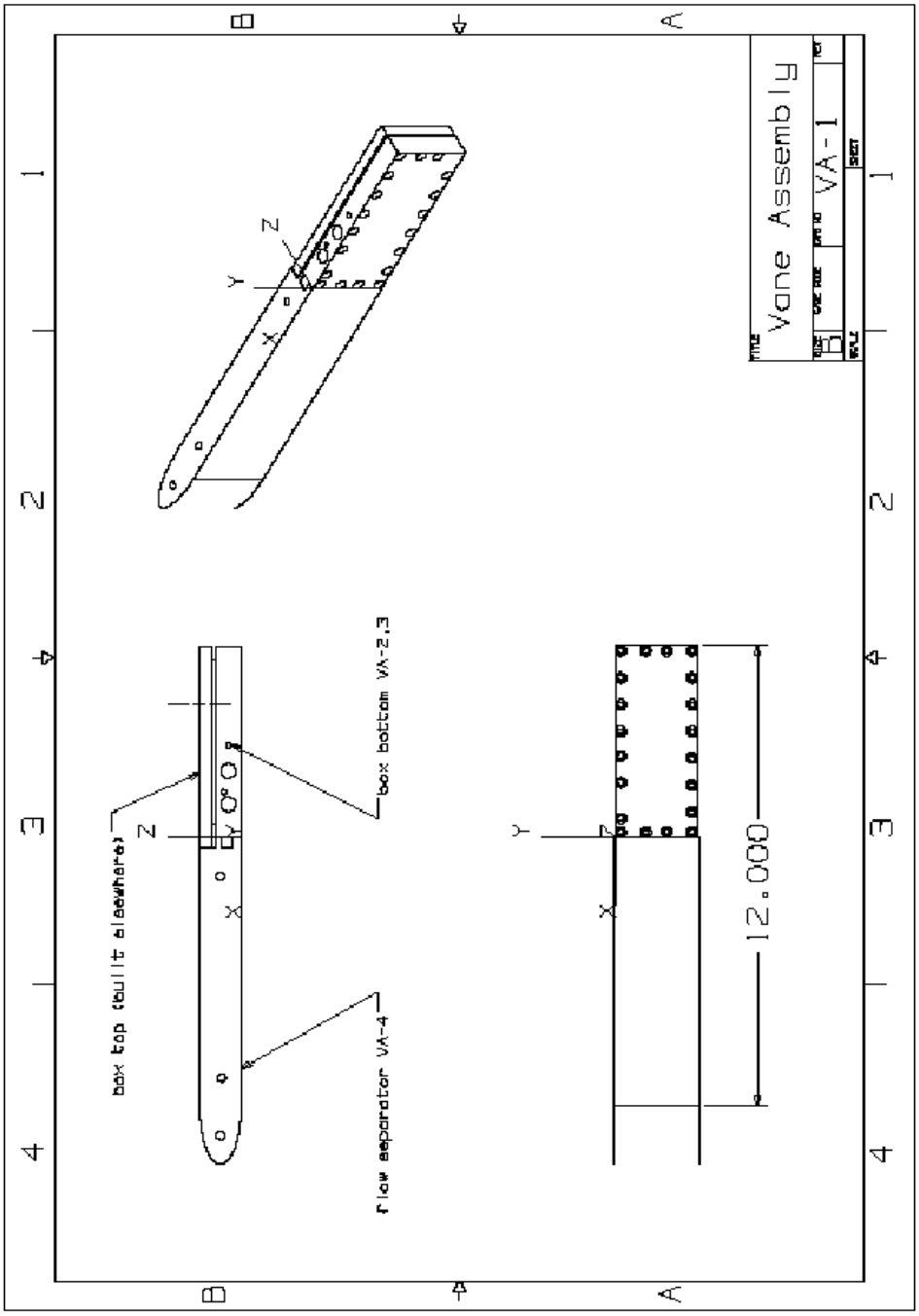
Vane Assembly
VA-1
box top (built elsewhere)
box bottom VA-2,3
flow separator VA-4
12.000

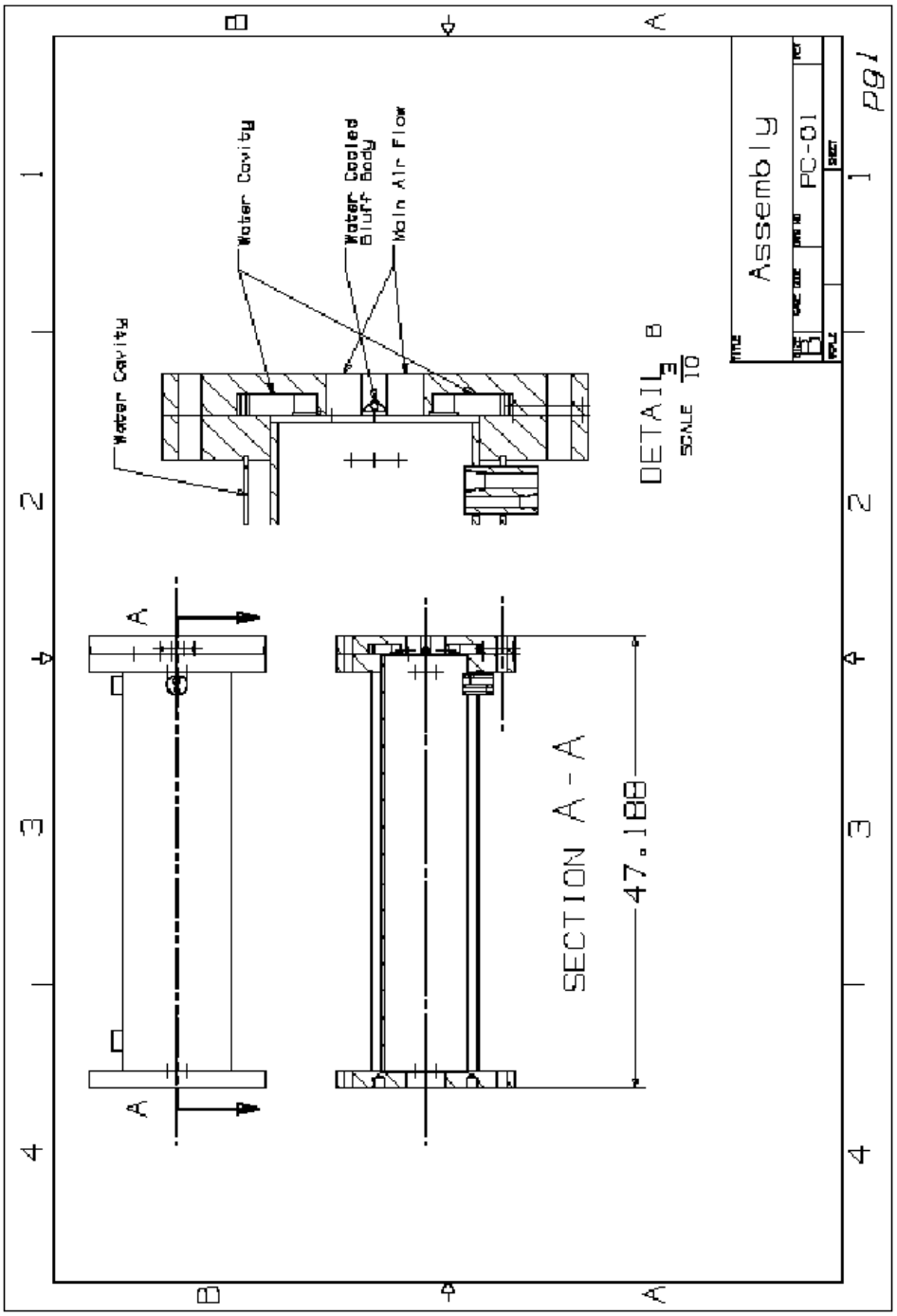
Water Cavity
Water Cooled Bluff Body
Main Air Flow
Water Cavity
DETAIL B
SCALE 3/10
SECTION A - A
47.188
Assembly
PC-01
pg1

Appendix C: Measurement System Details

Hardware

Item	*Manufacturer*	*Model Number*
Phase Doppler analyzer	Dantec Measurement Tech.	5500A-00 system
PDA processor	Dantec Measurement Tech.	58N-10 processor
Laser	Ion Laser Technology	5500-A-00
Power Supply	Ion Laser Technology	5405A-210-00
PIV camera (1)	Vision Research	Phantom v4
PIV camera (2,3)	IDT	X-Stream: XS-3 and XS-5
PIV laser (15 Hz)	New Wave Research	Solo-III
High rep PIV laser	Dantec	high rep Nd:Yag
DAQ board	National Instruments	NI-6251
Timing Hub	IDT	X-Stream

Software

Process	*Company*	*Software*
Camera/laser control	IDT	X-vision
Camera/laser control	National Instruments	LabView
Image Processing	Image Magick Studio	Image Magick
PIV	Aeroprobe	FlowIQ
Interpretation/Demonstration	Tecplot Inc.	Tecplot
Interpretation/Demonstration	Mathworks	Matlab
Calculation	Python	Python

Appendix D: Penetration Height and Core Location Identification

The following the program used to identify the spray penetration height. The program is broken up in input and script files.

Input File

```
%%%%%%%%%%%%%%%%%%%%%%%%%%%%%%%%%%%%%%%%%%%%%%%
"""Inputs for InstProc"""

def Inputs(inin=0):
    "File base name"
    baseName='W_V100_T070_q12_'
    "Locations of files"
    #tif directory
    tifDir='C:\\PIV_thesis\\W_V100_T070_q12\\tif\\'
    #PIV directory
    pivDir='C:\\PIV_thesis\\W_V100_T070_q12\\PIV\\'
    #Output directory
    writeDir='C:\\PIV_thesis\\W_V100_T070_q12\\output\\'
    "program parameters"
    #number of images to average
    Nimage_max=1169.
    "Laser/Camera systems parameters"
    #Physical Resolution (m/pixel)
    Res=44e-6
    #Pulse Separation
```

```
dt_pulse=2e-6
#Sampling frequency
f_smpl=15.
#fstop
F=6.
"FlowIQ parameters"
#mesh size
Nx=16.
Ny=8.
#window size
Wx=64.
Wy=32.
#peak detection
peakDetection='ThreePoint'
#interpolation shceme
interp='FFTnormFast'
"Interrogation parameters"
Xo=-0.03*0.254  #[m]
Zo=0.           #[m]
Xf=1.5*0.254    #[m]
Zf=0.02         #[m]
Yo=0.           #[m]
"User set limits"
Xmin=0.3*0.0254  #[m]
Xmax=1.5*0.0254  #[m]
Umin=5.         #[m/s]
Umax=130.       #[m/s]
Vmin=-50.       #[m/s]
Vmax=50.        #[m/s]
MinPen=15       #pixels
```

```
    return
{'baseName':baseName,'tifDir':tifDir,'pivDir':pivDir,'writeDir':writeDir,'Res':Res,'dt_puls
e':dt_pulse,'f_smpl':f_smpl,'F':F,
        'Nx':Nx,'Ny':Ny,'Wx':Wx,'Wy':Wy,'peakDetection':peakDetection,'interp':interp,'
Xo':Xo,'Zo':Zo,'Xf':Xf,'Zf':Zf,'Yo':Yo,
        'Xmin':Xmin,'Xmax':Xmax,'Umin':Umin,'Umax':Umax,'Vmin':Vmin,'Vmax':Vma
x,'MinPen':MinPen}
%%%%%%%%%%%%%%%%%%%%%%%%%%%%%%%%%%%%%%%%%%%%%%%%%%%%%%%%%%%%%%%%
```

Script File

```
%%%%%%%%%%%%%%%%%%%%%%%%%%%%%%%%%%%%%%%%%%%%%%%%%%%%%%%%%%%%%%%%
""" This program will map all of the instantaneous spray
characterisitcs of a jet in crossflow"""

import os, sys, csv
import numarray, Image, ImageStat
from numarray import *
from Scott import Input

"Run input file"
Ins=Input.Inputs()

"Get list of PIV and tif file names"
tifNames=os.listdir(Ins['tifDir'])
pivNames=os.listdir(Ins['pivDir'])

"""Start loop to examine PIV files"""
os.chdir(Ins['pivDir'])
"open first file to get pic info"
fPIV=open(Ins['pivDir']+pivNames[0],'r')
#read in header
header_filetype=fPIV.readline()
```

```
header_variables=fPIV.readline()
header_zone=fPIV.readline()
#get number of x and z values
ii=int(header_zone.split()[1][2:])
jj=int(header_zone.split()[2][2:])
#get X and Z positions
XZs=[]
for thisline in fPIV.readlines():
   XZs.append(map(float,thisline.strip().split())[0:2])
XZ=array(XZs)
XminArg,XmaxArg=argmin(abs(XZ[:ii,0]-Ins['Xmin'])),argmin(abs(XZ[:ii,0]-
Ins['Xmax']))
X=XZ[XminArg:XmaxArg,0] ### written to file *_X.txt
Z=XZ[arange(0,jj*ii,ii),1]
ZminArg,ZmaxArg=argmin(abs(Z-Ins['Zo'])),argmin(abs(Z-Ins['Zf']))
Z=Z[ZminArg:ZmaxArg] ###written to file *_Z.txt
dX=X[2]-X[1]
#initialize variables
kk,nn,t=0,0,0.0
VelSum=zeros([len(X),len(Z),2],'d')
VelCount=zeros([len(X),len(Z),2],'d')
Pen,Pen95=ones([len(pivNames),len(X)],'d'),zeros([len(pivNames),len(X)],'d')
Core,Core95=zeros([len(pivNames),len(X)],'d'),zeros([len(pivNames),len(X)],'d')
tconv,tconv=zeros([len(pivNames),len(X)],'d'),zeros([len(pivNames),len(X)],'d')

"loop through files"
for pivName in pivNames:
   #read in file
   fPIV=open(Ins['pivDir'] + pivName,'r')
   #read in header
   header_filetype=fPIV.readline()
```

```
    header_variables=fPIV.readline()
    header_zone=fPIV.readline()
    #read U,V
    listPIV=[]
    for thisline in fPIV.readlines():
        listPIV.append(map(float,thisline.strip().split())[2:4])
    listPIV=array(listPIV,'d')
    UU=[]
    "loop through x distance in single image"
    for i in arange(XminArg,XmaxArg):
        "get velocity sum and count for average velcity field and penetration"
        #loop through z distances
        UatX=zeros(ZmaxArg-ZminArg)
        for j in arange(ZminArg,ZmaxArg):
            if Ins['Umin']<listPIV[i+j*ii,0]<Ins['Umax']:
                VelSum[i-XminArg,j-ZminArg,0]=VelSum[i-XminArg,j-
ZminArg,0]+listPIV[i+j*ii,0]
                VelCount[i-XminArg,j-ZminArg,0]=VelCount[i-XminArg,j-ZminArg,0]+1
                #count in z direction to calculate penetration
                Pen[nn,i-XminArg]=Pen[nn,i-XminArg]+1
                UatX[j]=listPIV[i+j*ii,0]
            else:
                listPIV[i+j*ii,0]=listPIV[i+(j-1)*ii,0]
                UatX[j]=1000
            if Ins['Vmin']<listPIV[i+j*ii,1]<Ins['Vmax']:
                VelSum[i-XminArg,j-ZminArg,1]=VelSum[i-XminArg,j-
ZminArg,1]+listPIV[i+j*ii,1]
                VelCount[i-XminArg,j-ZminArg,1]=VelCount[i-XminArg,j-ZminArg,1]+1
            else:
                listPIV[i+j*ii,1]=listPIV[i+(j-1)*ii,1]
        Pen[nn,i-XminArg]=Pen[nn,i-XminArg]*Ins['Res']*Ins['Ny']
        "find core height"
```

```
        kk=Pen[nn,i-XminArg]/Ins['Res']/Ins['Ny']
        #average out velocity field to yeild more stable results
        UatXsmooth=zeros(len(UatX)-4)
        for k in arange(len(UatX)-4):
            UatXsmooth[k]=sum(UatX[k:k+4])
        Core[nn,i-XminArg]=(argmin(UatXsmooth)+2)*Ins['Res']*Ins['Ny']
    "loop counter"
    nn=nn+1
    print 'PIV-'+ str(nn)
"Analyze results and get final answers"
#write X and Z values
fWrite=open(Ins['writeDir']+Ins['baseName']+'X.txt','w')
writer=csv.writer(fWrite)
writer.writerow(X)
fWrite.close()
fWrite=open(Ins['writeDir']+Ins['baseName']+'Z.txt','w')
writer=csv.writer(fWrite)
writer.writerow(Z)
fWrite.close()
#calculate and write Uavg and Vavg velocity fields
for i in arange(size(VelCount,0)):
    for j in arange(size(VelCount,1)):
        for dir in [0,1]:
            if VelCount[i,j,dir]<1:
                VelCount[i,j,dir]=1
VelAvg=VelSum/VelCount
fWrite=open(Ins['writeDir']+Ins['baseName']+'Uavg.txt','w')

writer=csv.writer(fWrite)
writer.writerows(VelAvg[:,:,0])
fWrite.close()
```

```
fWrite=open(Ins['writeDir']+Ins['baseName']+'Ucount.txt','w')
writer=csv.writer(fWrite)
writer.writerows(VelCount[:,:,0])
fWrite.close()
fWrite=open(Ins['writeDir']+Ins['baseName']+'Vavg.txt','w')
writer=csv.writer(fWrite)
writer.writerows(VelAvg[:,:,1])
fWrite.close()
fWrite=open(Ins['writeDir']+Ins['baseName']+'Vcount.txt','w')
writer=csv.writer(fWrite)
writer.writerows(VelCount[:,:,1])
fWrite.close()
#calculate an average droplet residence time and write to file
dt,tconv=[],[]
for i in arange(size(VelAvg,0)):
   dt.append(dX/(sum(VelAvg[i,:,0])/(ZmaxArg-ZminArg)))
   tconv.append(sum(dt))
tconv=array(tconv)
fWrite=open(Ins['writeDir']+Ins['baseName']+'tconv.txt','w')
writer=csv.writer(fWrite)
writer.writerow(tconv)
fWrite.close()
#calculate and average and 95% confidence interval for Penetration and write to files
PenBar=sum(Pen,0)/size(Pen,0)
Pen95=[]
for i in arange(size(Pen,1)):
   PenRes=[]
   for n in arange(size(Pen,0)):
      PenRes.append(Pen[n,i]-PenBar[i])
   Pen95.append(2.*array(PenRes).stddev())
fWrite=open(Ins['writeDir']+Ins['baseName']+'Pen.txt','w')
```

```
writer=csv.writer(fWrite)
writer.writerows(list(Pen))
fWrite.close()
fWrite=open(Ins['writeDir']+Ins['baseName']+'PenBar.txt','w')
writer=csv.writer(fWrite)
writer.writerows([PenBar])
fWrite.close()
fWrite=open(Ins['writeDir']+Ins['baseName']+'Pen95.txt','w')
writer=csv.writer(fWrite)
writer.writerows([Pen95])
fWrite.close()
#calculate average ad 95% confidence interval for Core trajectory and write to files
CoreBar=sum(Core,0)/size(Core,0)
Core95=[]
for i in arange(size(Core,1)):
   CoreRes=[]
   for n in arange(size(Core,0)):
      CoreRes.append(Core[n,i]-CoreBar[i])
   Core95.append(2.*array(CoreRes).stddev())
fWrite=open(Ins['writeDir']+Ins['baseName']+'Core.txt','w')
writer=csv.writer(fWrite)
writer.writerows(list(Core))
fWrite.close()
fWrite=open(Ins['writeDir']+Ins['baseName']+'CoreBar.txt','w')
writer=csv.writer(fWrite)
writer.writerows([CoreBar])
fWrite.close()
fWrite=open(Ins['writeDir']+Ins['baseName']+'Core95.txt','w')
writer=csv.writer(fWrite)
writer.writerows([Core95])
fWrite.close()
```

Appendix E: Mass Fluctuation Program

The following the program used to identify the streamwise variation of average mass flux. The program is the same input file as the penetration/core program.

Mass Fluctuation program

```
%%%%%%%%%%%%%%%%%%%%%%%%%%%%%%%%%%%%%%%
 """Program will analyze the intensity fluctuations of the tif images in the
streamwise direction"""

from numarray import *
import os, sys, csv
import numarray, Image, ImageStat
from Scott import Input

"Run input file"
Ins=Input.Inputs()

########################################################################
########################
"unsteady fft function"
"unsteady fft using Lomb Periodogram"
def ufft(Tu,tifXu):

    #initialize variables
    PIu,frequ=[],[]
    N,R,Var,Sint,Cost,tau,t,Rcos,Cos2,Rsin,Sin2=[0]*11
    #define population statistics
    "temp"
```

```
    N=len(tifXu)
    R=tifXu-tifXu.mean()
    Var=1./(N-1.)*sum(R**2)
    # frequency limits and steps
    fmin,fmax,fstep=1000,3000,20
    omega=arange(fmin,fmax,fstep)*2.*pi
    for w in omega:
        #calculate offset
        Sint=sum(sin(2.*w*Tu))
        Cost=sum(sin(2.*w*Tu))
        tau=1./2./w*arctan(Sint/Cost)
        t=Tu-tau
        #calculate spectral power at w
        Rcos=(sum(R*cos(w*t)))**2
        Cos2=sum((cos(w*t))**2)
        Rsin=(sum(R*sin(w*t)))**2
        Sin2=sum((sin(w*t))**2)
        PIu.append(1./2./Var*(Rcos/Cos2+Rsin/Sin2))
        frequ.append(w/2./pi)
    return PIu,frequ
##############################################################################
############################

"load needed information from InstProc"
#x values in interogation area
fX=open(Ins['writeDir']+Ins['baseName']+'X.txt','r')
x=map(float,fX.readline().strip().split(','))
#average velocity field in interrogation area
fUavg=open(Ins['writeDir']+Ins['baseName']+'Uavg.txt','r')
Uavg_i=[]
for thisline in fUavg.readlines():
```

```
    Uavg_i.append(map(float, thisline.strip().split(',')))
#velocity count in iterrogation area
fUcount=open(Ins['writeDir']+Ins['baseName']+'Ucount.txt','r')
Ucount=[]
for thisline in fUcount.readlines():
    Ucount.append(map(float, thisline.strip().split(',')))
#calculated residence time in interogation area
ftconv=open(Ins['writeDir']+Ins['baseName']+'tconv.txt','r')
tconv=array(map(float,ftconv.readline().strip().split(',')))

"derive experimental parameters needed"
#average velocity field with significant count
Upass=[]
CountMin=max(max(Ucount))*.45
for xUcount in Ucount:
    Upass.append(map(lambda x: x>(CountMin) and 1 or 0,xUcount))
Uavg=array(Uavg_i)*array(Upass)
#calculate the initial velocity
Uo_int=Uavg[0:4,:].mean()
Uo_fin=Uavg[0:-5,:].mean()
#calculate average acceleration
aLC=1/(2*x[0])*(Uo_int**2)
aSP=1/(2*(x[-1]-x[0]))*(Uo_fin**2-Uo_int**2)
#let Uo total equal zero at the orifice


"load pictures and evaluate the fluxuation of mass over the streamwise location"
#load tif names
os.chdir(Ins['tifDir'])
tifNames_all=os.listdir(Ins['tifDir'])
tifNames=[]
```

```
for nfile in arange(0,len(tifNames_all),10):
   tifNames.append(tifNames_all[nfile])
##tifNames=[tifNames_all[1]]
#initialize variables
mm=0
InstFreq,PI,PIs,freq,freqs,tifXs,Ts=[],[],[],[],[],[],[]
PIcohs=[]
"Start Loop"
qq=0
for tifName in tifNames:
   #initialize loop variables
   tifX,freq,PIwin=[],[],[]
   #load image
   tif_raw=Image.open(tifName)
   #basic threshold of image
   tif=tif_raw.point(lambda i: i-ImageStat.Stat(tif_raw).mean[0])
   #some intensities over Z direction
   for i in arange(tif.size[0]):
      #define box edges
      left=i
      right=i+15#Ins['Nx']-1
      top=0
      bottom=tif.size[1]
      #find intensity of slice
      tifX.append(ImageStat.Stat(tif.crop([left,top,right,bottom])).mean[0])
   #calc position, X, over the entire picture
   X=Ins['Res']*arange(tif.size[0])
   Xo=argmin(abs(X-x[0]))
   #calc time at each
   #pixel based on acceleration, an initial liquid phase velocity of zero and acc
   TLC=(2*aLC*X[:int(Xo)])**.5/aLC
```

```
    TSP=(-Uo_int+(Uo_int**2+2*aSP*X[int(Xo):])**.5)/aSP
    T=concatenate([TLC,TSP+max(TLC)-min(TSP)])[100:-21]
    tifX=array(tifX[100:-21])
    tifXs.append(tifX)
    PIwin=[]
##    for io in arange(0,len(T)-(len(T)%400),125):
##        ii=io+len(tifX)%500
##        T_loop=T[ii:ii+500]
##        tifX_loop=tifX[ii:ii+500]
##
##        #take unsteady fft
##        [PIiwin,fi]=ufft(T_loop,tifX_loop)
##        PIwin.append(PIiwin)
##    PIcoh=product(PIwin[1:-1],0)
##    PIcoh=PIcoh/PIcoh.max()
##    PIi=PIcoh*PIwin[int(size(PIwin,0))/2]
    [PIi,fi]=ufft(T,tifX)
    PIs.append(PIi)
##    PIcohs.append(PIcoh)
    del(tif)
    qq=qq+1
    print qq

fWrite=open(Ins['writeDir']+Ins['baseName']+'PIcohs.txt','w')
writer=csv.writer(fWrite)
writer.writerows(PIcohs)
fWrite.close()
fWrite=open(Ins['writeDir']+Ins['baseName']+'PIs.txt','w')
writer=csv.writer(fWrite)
writer.writerows(PIs)
fWrite.close()
```

```
fWrite=open(Ins['writeDir']+Ins['baseName']+'freq.txt','w')
writer=csv.writer(fWrite)
writer.writerow(fi)
fWrite.close()
fWrite=open(Ins['writeDir']+Ins['baseName']+'tifXs.txt','w')
writer=csv.writer(fWrite)
writer.writerows(tifXs)
fWrite.close()
fWrite=open(Ins['writeDir']+Ins['baseName']+'T.txt','w')
writer=csv.writer(fWrite)
writer.writerow(T)
fWrite.close()

raw_input('hit enter')
```

Appendix F: Data Collection and Processing

Summary

PIV Experimental Conditions and Interrogation Regions

Case	*Liquid*	*Air Velocity*	*Air Temp*	*Momentum Ratio*	*Regions*	*Depth*
		U_o = [ft/s]	T = [F]	j		[in]
1	water	245	70	12	A	0
2	water	328	70	12	A	0
3	water	450	250	12	A	0
4	water	450	250	18	A	0
5	water	450	900	12	A,B,C,D	0
6	water	450	900	12	A,B,C,D	3/16
7	water	450	900	12	A,B,C,D	-3/16
8	water	450	900	12	A,B,C,D	3/8
9	water	450	900	18	A,B,C,D	0
10	water	450	900	18	B,C,D	3/16
11	water	450	900	18	A,B,C,D	3/8
12	water	450	900	18	A	-3/16
13	water	450	900	12	8kHz	0
14	kerosene	450	250	12	A,B,C,D	0
15	kerosene	450	250	18	A,B,C,D	0
16	kerosene	450	900	7	α, β, γ,δ	0
17	kerosene	450	900	12	α,β,γ,δ	0
18	kerosene	450	900	18	α,β,γ,δ	0
19	kerosene	450	900	28	α,β,γ,δ	0

PDA Experimental Conditions

Case	*Liquid*	*Air Velocity*	*Air Temp*	*Momentum Ratio*	*# of Points*
		ft/s	F		
1	kerosene	450	250	12	106
2	kerosene	450	250	18	106
3	kerosene	450	900	12	106
4	kerosene	450	900	18	106

PIV Processing

Case	*Region*	*Depth*	*Inst. Velocity*	*Time-avg. Velocity*
5	A	0	yes	yes
6	A	3/16	yes	no
8	A	3/8	yes	no
5	B	0	yes	yes
6	B	3/16	no	yes
8	B	3/8	yes	yes
7	B	-3/8	no	no
5	C	0	yes	yes
6	C	3/16	yes	yes
8	C	3/8	yes	yes
5	D	0	no	yes
6	D	3/16	yes	yes
8	D	3/8	yes	yes
9	A	0	yes	yes
11	A	3/8	yes	yes
12	A	-3/16	no	no
9	B	0	yes	yes
10	B	3/16	yes	yes

Case	*Region*	*Depth*	*Inst. Velocity*	*Time-avg. Velocity*
11	B	3/8	yes	yes
9	C	0	yes	yes
10	C	3/16	yes	yes
11	C	3/8	yes	yes
9	D	0	yes	yes
10	D	3/16	yes	yes
11	D	3/8	yes	no
3	A	0	no	no
13	8kHz	0	no	no
2	A	0	no	no
1	A	0	no	no
14	A	0	yes	yes
14	B	0	yes	yes
14	C	0	yes	yes
14	D	0	yes	yes
15	A	0	yes	yes
15	B	0	yes	yes
15	C	0	yes	yes
15	D	0	yes	yes
16	α	0	yes	yes
16	β	0	yes	yes
16	γ	0	yes	yes
16	δ	0	yes	no
17	α	0	yes	yes
17	β	0	yes	yes
17	γ	0	yes	yes
17	δ	0	yes	no
18	α	0	yes	yes
18	β	0	yes	yes

Case	*Region*	*Depth*	*Inst. Velocity*	*Time-avg. Velocity*
18	γ	0	yes	yes
18	δ	0	yes	yes
19	α	0	yes	yes
19	β	0	yes	yes
19	γ	0	yes	yes
19	δ	0	yes	yes

Appendix G: Data Collection Process

PIV System Measurement Instructions

Laser/mirrors hook up, startup, shutdown
Double ruby laser
High rep laser

Camera hook up, startup, shutdown

Computer/Trigger hookup

Software startup, config
Double ruby laser trigger settings
High rep laser trigger settings
Camera settings

Window installation, cleaning, properties

Laser hookup – double ruby laser
Dual Laser

1. Plug wires from laser into plug labeled main umbilical on controller.
2. Plug controller into outlet. (make sure shutter on laser is closed, small tab on top of outlet)

Mirrors Setup

1. Make sure mirrors are in about the right position.
   a) After the laser exit place a 90deg mirror pointed up and then one 90deg mirror pointed towards the experiment.
   b) After the 90 deg mirrors place be a lens to refocus the beam and then a cylindrical beam to spread the the beam into a sheet.
   c) Just above the experiment place a larger 90deg mirror to deflect the sheet into the experiment
2. Turn laser on (key and I/O button on back), then press start/standby for 3 seconds
3. Set laser to internal and low intensity on controller, and turn laser on (buttons labeled laser)
4. Adjust 90deg mirrors the the beam it hitting approximately the center of each
5. Then with then with either goggles or a sheet of paper move the focal lens so that the total laser path up to that point is 3 ½ ft.

6. Then find the focal point in the beam past the **f**ocal lens (between 3-10), and place the cylindrical lens about 2 or 3 inches past the focal point.
7. Now line up the big 90deg mirror so that the laser sheet falls on the centerline of the experiment.
    a) moving the mirror away and towards the beam for gross adjustment in the depth direction
    b) moving the mirror up and down for minor adjustment in the depth direction (a and b should be used in conjunction to get the laser sheet to hit the center of the mirror vertically)
    c) swinging the mirror CW and CCW to make the laser sheet parallel to the experiment walls in the flow direction
8. Placing a sheet of paper just in front of the big 90deg mirror or using goggles to identify the spacial gradient of the laser across the mirror. Move the mirror and the mirrors in the flow direction to that the center point of the laser intensity hits the center of the mirror and is approximately in the center of the current measurement plane.
9. Check to make sure all mirrors and lenses are perpendicular to laser beam path by eye.
10. Move cylindrical lens back and forth in the laser path direction while watching the laser sheet reflection inside the experiment. Adjust lens until laser sheet is minimum thickness (about 1mm or jet orifice diameter)
11. Now adjust the focal lens to further optimize the laser sheet thickness
12. Adjust the cylindrical lens in the direction perpendicular to the beam path by spinning it it on its stand by a few degrees. If the lens is not aligned the beam will look like this:

13. Fine tune the height of the large 90deg mirror so the beam is centered on the measurement plane desired.
14. Turn laser on standby or close shutter

Laser/Mirrors Shutdown

1. Turn laser on standby then turn off power switch on controller
2. Cover all mirror with plastic bags or bubble wrap

Camera hookup, startup, shutdown

Hookup/Startup

1. Attach appropriate lenses, reversing rings, and spacers.
2. Plug in camera power adapter.
3. Plug in power cord to camera (red dots match up) (power cord should always be first to make sure camera is grounded).
4. Plug USB and BNC cords to camera BNC connects to plug labeled Sync In.
5. Plug USB into computer and BNC into trigger.
6. Start up computer then turn on camera.

Shutdown

1. Turn off camera.
2. If unplugging make sure to unplug power last (to keep camera grounded)
3. Put on lens cap

Trigger hookup

Double ruby laser

1. Turn on computer and start up trigger controller (XVision -> tool -> timing controls)
2. Plug BNC into channel labeled flash lamp 1 in software (currently ch 2) and into the top BNC plug labeled Fire Lamp on the laser controller.
3. Plug BNC into channel labeled q-switch 1 in software (currently ch 3) and into the top BNC plug labeled Fire q-switch on the laser controller.
4. Plug BNC into channel labeled flash lamp 2 in software (currently ch 4) and into the bottom BNC plug labeled fire lamp on the laser controller.
5. Plug BNC into channel labeled q-switch 2 in software (currently ch 5) and into the bottom BNC plug labeled fire q-switch on the laser controller.
6. Take BNC cable plugged into camera and plug it into the channel labeled camera 1 (currently ch 6)
7. Plug in the USB plug from the trigger to the computer.
8. On laser controller turn both lasers to external.

Camera startup and config

Startup

1. Make sure the laser is on, set on standby, and set on external.
2. Make sure the camera is plugged in and turned on.
3. Turn on or restart Xstream program.
4. Go to general options --> frame info --> check time and date
5. Go to the tools menu --> timing control.
6. Press the camera icon in the task bar at the top.
    a) hit next, camera(s) should show up in list, continue through menus
    b) if camera does not show up check USB plugs and camera power, then restart the program and possible the computer

Trigger config

1. Check timing settings
    a) General tab:
        - Internal Frequency: 15006
        - Ext. Trig A Frequency: unchecked
        - Ext. Trig B Frequency: unchecked
    b) 0
        - Label: frame rate 1
        - Mode: Internal
        - Invert output: unchecked
        - Gate: None
        - Invert Gate: unchecked
        - Output Divider 1: 1000
        - Duty Cycle: 100
        - Output Delay: 0.00
    c) 1
        - Label: frame rate 2
        - Mode: Internal
        - Invert output: unchecked
        - Gate: None

- Invert Gate: unchecked
- Output Divider 1: 1000
- Duty Cycle: 100
- Output Delay: 2.00

d) 2

- Label: 1 flash
- Mode: Burst
- Trigger: Output 0
- Output Divider1: 15
- Duty Cycle: 100
- Pulses: 1
- Output Delay: 0.00

e) 3

- Label: 1 qswitch
- Mode: Burst
- Trigger: Output 0
- Output Divider1: 15
- Duty Cycle: 100
- Pulses: 1
- Output Delay: 190.00

f) 4

- Label: 2 flash
- Mode: Burst
- Trigger: Output 1
- Output Divider1: 15
- Duty Cycle: 100
- Pulses: 1
- Output Delay: 0.00

g) 5

- Label: 2 qswitch
- Mode: Burst

- Trigger: Output 1
- Output Divider1: 15
- Duty Cycle: 100
- Pulses: 1
- Output Delay: 190.00

h) 6

- Label: camera
- Mode: Burst
- Trigger: Output 0
- Output Divider1: 15
- Duty Cycle: 190
- Pulses: 1
- Output Delay: 1.00

i) 7

- Label: camera2
- Mode: Burst
- Invert output: unchecked
- Trigger: Output 0
- Invert Gate: unchecked
- Output Divider 1: 15
- Duty Cycle: 190
- Output Delay: 1.00

2. In timing control, check all boxes on left.
3. In timing control, press general on/off to on (on left), and local on/off to on (on right) for any of the checked channels.
   a) If lasers on are (two laser buttons above standby/on button) and controller is set to external, the laser should now flash.
4. Place camera in position facing the laser. An image should appear (may be out of focus or blinking)

Camera settings

1. Check camera setting (on left), settings change at every restart.

a) Camera Tab
   - Sensor Gain: No Gain
   - Rate: 15 Hz
   - Exp: Leave as is
   - Binning: 1x1
   - Pixel Depth: 8 Bit (upper)
   - Live Time Out[s]: leave as is
   - Exposure Mode: Double
   - [gear picture]: set folder and file names to save to

b) Record Tab
   - Record Mode: Normal
   - Frames: enter number of frames wanted (nominally 3000)
   - Frame Sync: External
   - Sync Cfg: Pulse High
   - Trigger Cfg: IRIG

2. Change camera settings on camera tab to single exposure and take calibration images of the ruler to get the magnification desired. Focus be set to a midrange value. When proper magnification is found measure distance from measurement plane to the front of the camera box. Make sure image is in focus.
3. Place camera facing experiment, change camera setting back to double exposure, and press the play button.
   a) if image is flashing on and off or bright and dark, double check camera and laser settings.
   b) if images are drastically light then dark, change laser delay, second trigger channel (currently ch1).
   c) if images are slightly light then dark check to make sure laser intensity profile is center on mirror.
4. If experiment is not currently running for other reasons, it should be turned on now.
5. Line up camera to a position that has a consistent, even reflections.
6. Set camera facing experiment at the distance measure in calibration.
   a) Adjust f-stop ring so that the imaging is a little dim (easier to focus if image is dim).

b) Gross focus adjustment by moving the camera and then after acceptable then using focus ring to fine tune focus. Focus should be moved as little as possible to keep calibration valid.

7. Move camera to measurement plane and everything is ready for measurements.

Window installation, cleaning, properties

Installation

1. If not already cut/attached, take a piece for coated fiberglass tubing (orange coating) and cut a piece slightly longer then the material needed to wrap tube around the inside of the SS window frame piece. Then cut the fiberglass tube lengthwise.
2. Cut slits into the short direction where the fiberglass folds into the corners of the frame. Then take the fiberglass and for wrap it around the window frame so that the metal-metal surface is completely covered by the fiberglass with no extra and the cloth side is touching the experiment wall. The coating and ends of the piece of the fiberglass should be facing away from the center of the window frame.
3. Then take smaller/scrap pieces of fiberglass and tie them around the corners so there is some extra thickness to the fiberglass in the corners and to hole the main piece of fiberglass to the window frame.
4. Place the glass on the side of the window frame with the longer/extra fiberglass so the window is touching the white/cloth side of the fiberglass. Then wrap the fiberglass around the window and attach the four pieces to hold the window to the frame. Tighten the screws so that the pieces don't move, but minimum force is required to turn the screws.
5. Now the fiberglass should start parallel to the bottom of the window frame, then wrap around the inside of the metal window frame and outside of the glass in an S shape.
6. Attach the window frame the experiment and retighten screws that are holding the window to the frame.
7. After experiment is started, check for leaks and tighten screws appropriately.

Cleaning

1. Loosen all of the screws holding the window to the window frame.
2. Completely unscrew the bottom piece holding the window on (make sure to keep some pressure on the window to make sure it doesn't fall out).
3. Slide the window down, loosening screws as necessary.
4. Clean windows using water and paper towels initially, then use aerosol, ammonia based cleaner and lens sheets.
5. Make sure to also clean the white/cloth side of the fiberglass on the bottom of the window with cleaner also, so the fiberglass does not dirty the window while replacing it.
6. Slide widow back into place making sure that the window is covering fiberglass on all four corners. Then lightly tighten the screws on the side to hold the window.

7. Replace the bottom widow holder and lightly tighten screws. After experiment is back on tighten screws as needed to stop leaks.

Properties

Currently we have three materials for the windows

1/4" th Quartz/Vicor windows are proper for operating temperatures up to 1300 -1500 deg F.

1/4" th Pyrex windows are proper for operating temperature up to 400-500 deg F

Appendix H: Summary of Previous Work

years	Investigator	Associates	Jet Segment	Measurement Techniques	Topics Covered
1972, 74, 75, 77, 79	Schetz	Kush, Joshi, McVey, Padhye, Baranowsky	liquid column and near field spray	instantaneous and streak photography	effects of injector shape/size, injector orientation and angle, and liquid properties on penetration, column breakup
1981, 82, 83, 84, 86, 89	Schetz	Nejad, Less, Nejad, Ogg, Hewitt, Kavsaoglu	liquid column and near field spray	instantaneous photography and Fraunhofer diffraction	measurement and correlation of column breakup characteristics, time-resolved measurements of surface instabilities and droplet SMD fluctuations
1985	Ingebo	n/a	far field spray	scanning radiometer	correlation of droplet diameter to Weber and gas-Reynolds number
1992	Nguyen	Karagozian	liquid column	theoretical modeling	trajectory and deformation of liquid column
1992, 94, 97	Nejad	Chen, Roe, Green, Elliott, Mosedale, Gruber, Carter	liquid column, near and far fields	PDA, PIV	correlation of droplet size, velocity field, spray height, to flow parameters
1997, 98	Wu	Kirkendall, Fuller, Nejad	liquid column, far field	shadowgraph, PDA	correlation of trajectory and length to flow parameters, and velocity, size, and mass flux profiles of droplets
1997	Inamura	Nagai	liquid column, far field	instantaneous photography, PDA	description of liquid column breakup, and characterization of droplet distributions (size/velocity) correlated to flow parameters
2000	Zhang	Ziada	far field spray	PDA	characterization of droplet distributions (size/ mass flux) correlated to flow parameters
2000, 02	Becker	Hassa	liquid column, near and far field	shadow graphs, PDA	correlation of spray height in near field and droplet distributions in far field to flow parameters
2003	Madabhushi	n/a	liquid column, near and far field	computational modeling	comparison of computational model for predicting jet in crossflow behavior to existing data